2nd Advanced Optical Metrology Compendium

Advanced Optical Metrology

Geoscience | Corrosion | Particles | Additive
Manufacturing: Metallurgy, Cut Analysis & Porosity

EVIDENT
OLYMPUS

WILEY

**The latest eBook from
Advanced Optical Metrology.
Download for free.**

This compendium includes a collection of optical metrology papers, a repository of teaching materials, and instructions on how to publish scientific achievements.

With the aim of improving communication between fundamental research and industrial applications in the field of optical metrology we have collected and organized existing information and made it more accessible and useful for researchers and practitioners.

Layered Cathode Materials: Precursors, Synthesis, Microstructure, Electrochemical Properties, and Battery Performance

Bin Huang, Lei Cheng, Xinze Li, Zaowen Zhao, Jianwen Yang, Yanwei Li, Youyong Pang, and Guozhong Cao*

The exploitation of clean energy promotes the exploration of next-generation lithium-ion batteries (LIBs) with high energy-density, long life, high safety, and low cost. Ni-rich layered cathode materials are one of the most promising candidates for next-generation LIBs. Numerous studies focusing on the synthesis and modifications of the layered cathode materials are published every year. Many physical features of precursors, such as density, morphology, size distribution, and microstructure of primary particles pass to the resulting cathode materials, thus significantly affecting their electrochemical properties and battery performance. This review focuses on the recent advances in the controlled synthesis of hydroxide precursors and the growth of particles. The essential parameters in controlled coprecipitation are discussed in detail. Some innovative technologies for precursor modifications and for the synthesis of novel precursors are highlighted. In addition, future perspectives of the development of hydroxide precursors are presented.

1. Introduction

The applications of lithium-ion batteries (LIBs) have spread pervasively from consumer electronics (CEs) and portable electric tools to transportation sections and distributed energy storage devices due to their high energy density, high power density, long cycle life, and low self-discharge.[1] With the fast development of electric vehicles (EVs), demand for high-energy-density

B. Huang, X. Li, J. Yang, Y. Li, Y. Pang
Guangxi Key Laboratory of Electrochemical and
Magneto-chemical Functional Materials
College of Chemistry and Bioengineering
Guilin University of Technology
Guilin 541004, China
L. Cheng, Z. Zhao
School of Metallurgy and Environment
Central South University
Changsha 410083, China
G. Cao
Department of Materials Science and Engineering
University of Washington
Seattle, WA 98195, USA
E-mail: gzcao@u.washington.edu

The ORCID identification number(s) for the author(s) of this article can be found under https://doi.org/10.1002/smll.202107697.

LIBs is ever-growing. The driving mileage per charge of EVs and the cost of EV batteries remain unsatisfactory so far. In a battery, cathode is a limiting factor, and determines, to a large degree, the operation voltage and storage capacity.[2] The cost of cathode material accounts for ≈40% of overall cost in a battery cell.[3] Hence, development of cathode materials with high energy-density and low cost is the primary way to improve energy density and reduce cost for LIBs.

Ni-rich layered oxides, $LiNi_{1-x-y}Co_xM_yO_2$ (M = Mn, Al, etc.), possess high specific capacity (≈160–220 mAh g^{-1}, depend on Ni fraction) and become the most widely used cathode materials for high-energy-density LIBs.[4] The energy density of Ni-rich materials can be feasibly improved by increasing the Ni fraction in the materials, but at the cost of their structural stability, surficial stability, and safety.[5] In the past decades, great efforts have been devoted to solving the issues brought by high Ni content, including surface coating,[6] bulk doping,[7] synthesis of single crystal particles,[8] and combination of two or more strategies.[9] Benefiting from the intensive researches of cathode materials, Ni content in layered cathodes is gradually improved. Furthermore, industrialization of Co-free Ni-rich cathode materials is put on agenda.

Investigation on the precursors for synthesizing Ni-rich cathode materials is much limited, though it is well-known that precursors usually impact on the electrochemical performance of cathodes. Ni-rich cathode materials are mostly synthesized from hydroxide or carbonate precursors, $Ni_{1-x-y}Co_xM_y(OH)_2/Ni_{1-x-y}Co_xM_yCO_3$ (M = Mn, Al, etc.). Some physical features (e.g., particle size, microstructures, etc.) of the precursors can pass to the cathode materials, thus affecting Li$^+$ diffusion and internal strain in the cathode particles.[10]

It should be mentioned that the term "precursor" in the field of layered cathodes is more as an intermediate compound, deviating from more broadly and commonly used for molecules containing single metal elements. The precursors can also be regarded as preliminary products of layered cathodes. The chemical composition of a precursor is also the same as the final product except for the absence of lithium in the former and different anions in them. To obtain layered cathodes, the

precursors only need a calcination with lithium source. During calcination, the valences of the transition metals (TMs) usually rise (i.e., $Ni^{2+} \rightarrow Ni^{3+}$, $Co^{2+} \rightarrow Co^{3+}$, $Mn^{2+} \rightarrow Mn^{4+}$) in order to balance the change of anion groups (i.e., from $-(OH)_2/-CO_3$ to $-O_2$).[11] The change of anion groups during calcination is accompanied with the release of H_2O for hydroxide precursors or CO_2 for carbonate precursors, as well as the formation of pores.[11–12] As the mass fraction of anion groups in hydroxide precursors is lower than that in carbonate counterparts, hydroxides release less gas and can form more dense cathodes. Hence, hydroxide precursors are more attractive, and overwhelmingly dominate the field of layered cathodes.

This article provides a review of recent advances in controlled synthesis and modifications of precursors for layered cathode materials and the role of their microstructure in electrochemical performance of the final cathodes. In addition, perspectives on the development of Ni-rich precursors are presented.

2. Synthesis Methods

For synthesis of layered cathode materials, various methods have been developed and studied extensively, such as all-solid-state method,[13] sol–gel method,[14] spray-drying,[15] solvo/hydrothermal method,[16] and coprecipitation-calcination method.[17] The all-solid-state method is usually used to produce final cathodes in solid-state calcination (powder sintering) without preparing precursors. This method is simple and extremely easy to be scaled up. However, owing to the characteristics of powder mixing, the elements in the raw materials can hardly be mixed homogeneously at atomic level. Moreover, the products obtained by all-solid-state method have lower tap density due to their irregular particle morphology with particle size ranging from submicrometers to a few micrometers.

For the sol–gel method, spray-drying, solvo/hydrothermal method, and coprecipitation-calcination method, in fact, they are usually combined with a high-temperature solid-state lithiation. In other words, precursors are obtained at first, then converted into final cathodes by calcination. Sol–gel method is a wet chemical technique in which the reactants can be mixed homogeneously at atomic level. This is a major advantage of this method. Unfortunately, sol–gel method requires addition of organic acids as chelating agents (e.g., citric acid) and extra energy consumption for the solvent evaporation and gelation.[14a] Also, the material particles obtained by sol–gel method are sub-micrometers in size.[1a] In a typical spray-drying, a solution containing stoichiometric ratio of Li and TMs sources is prepared, followed by feeding into a spray dryer to form precursor powder with a spherical morphology. Then, the precursor is calcined at appropriate temperature to form final cathode.[15c] This method is simpler than sol–gel method and can achieve continuous production. However, the precursor will be too porous due to the fast evaporation of solvents during spray-drying. As a result, a high tap density cannot be guaranteed, and the morphology of the precursor will be probably changed during the calcination. For solvo/hydrothermal method, the morphology of the precursor can be easily controlled by adjusting the synthesis conditions (e.g. temperature, solvents, templates, etc.). For example, Zhang et al.[16a] prepared a $Ni_{0.8}Co_{0.1}Mn_{0.1}CO_3$

precursor composed of submicron primary particles by a urea-assisted hydrothermal method. The final $LiNi_{0.8}Co_{0.1}Mn_{0.1}O_2$ cathode made from this precursor showed near-nanograin size, which was able to alleviate the anisotropic volume change during charge–discharge cycles. Ryu et al.[16b] synthesized a dumbbell-like $Ni_{1/3}Mn_{1/3}Co_{1/3}CO_3$ precursor composed of nanocubes by a urea-assisted solvo/hydrothermal method. The final $LiNi_{1/3}Mn_{1/3}Co_{1/3}O_2$ cathode inherited the micrometer-sized dumbbell-like morphology and the nodular surface which could provide innumerable Li reaction site. As a result, the final cathode exhibited high initial discharge capacity, excellent cycling performance and rate capability. Although solvo/hydrothermal method can achieve controlled synthesis of precursors, they are not suitable for industrial production.

Coprecipitation method is used the most widely for preparing layered precursors. This method allows homogeneous mixing of elements, produces dense and narrowly distributed particles, and is suitable for scalable batch or continuous production, thus almost becoming the only choice in industry. As aforementioned, hydroxide precursors are more suitable for layered cathodes. Thus, the remainder of this article exclusively focuses on the hydroxide precursors. In general, hydroxide precursors are synthesized in a continuous stirred tank reactor (CSTR) using aqueous solutions of TM sulfates or nitrates as metal sources, a NaOH solution as precipitant and an NH_4OH solution as chelating agent. It is widely cognized that the composition, particle size, crystalline arrangement, structure ordering, and impurity content of cathode materials account for electrochemical performance, and largely depend on the precursors, which, in turn, depend on the reaction conditions in coprecipitation reactors.[18] Hence, the factors influencing the properties of hydroxide precursors include concentrations of the reactants, pH value, temperature, feed rate, stirring speed, and shapes of agitator blade and CSTR.[18a] As the factors influencing the microstructure of precursors are complex, controlled synthesis of desired precursors by coprecipitation is not easy. However, investigation focusing on the controlled coprecipitation is not intensive enough. Furthermore, industrial manufacturers of precursors are not as well-developed as their downstream industries, i.e., manufacturers of cathode materials, battery packs, and EVs. Taking China's precursor industry as an example, highly automated and intelligent manufactories have been spread from EV industry to battery industry, and thereafter to cathode material industry. As for precursor manufacturers, however, numerous nonstandard equipment, complicated processes, and inappropriate technique roadmap are adopted. Therefore, the lack of in-depth and systematic insight into the precursor synthesis has become an obstacle that impedes further development of precursor industry. For this reason, the following sections are focused on the advances in the controlled synthesis and modifications of hydroxide precursors by means of coprecipitation.

3. Controlled Particle Growth in Coprecipitation

Commercial Ni-rich hydroxide precursors are dense spherical particles with a diameter ranging from several micrometers to more than 10 μm, and are composed of nanoscaled primary
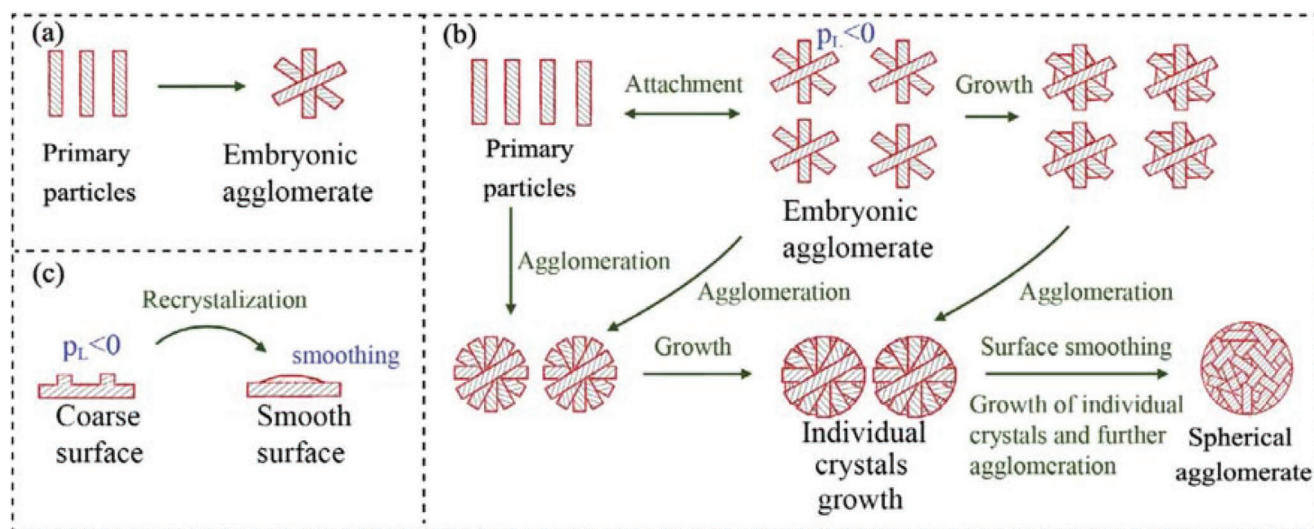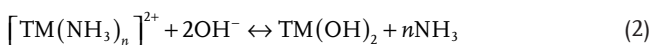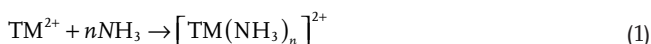
ADVANCED
SCIENCE NEWS
www.advancedsciencenews.com

NANO · MICRO
small
www.small-journal.com

Figure 1. Schematic illustrations of a) the formation of embryonic agglomerate, b) the formation of the secondary particles, and c) the mechanism of re-crystallization. Reproduced with permission.[20] Copyright 2015, Elsevier.

grains. In a typical coprecipitation process, precursor particles are formed under a mechanism described by Equations (1) and (2)[19]

$$TM^{2+} + nNH_3 \rightarrow \left[TM(NH_3)_n \right]^{2+} \tag{1}$$

$$\left[TM(NH_3)_n \right]^{2+} + 2OH^- \leftrightarrow TM(OH)_2 + nNH_3 \tag{2}$$

Obviously, there is a competing relationship between the formation of $[TM(NH_3)_n]^{2+}$ (complexation) and precipitation in a coprecipitation process, which engenders a dissolution-recrystallization mechanism, and makes the coprecipitation controllable. Based on the mechanism, the growth of hydroxide precursors can be divided into three main stages as follows.[20] First, at the beginning of the coprecipitation, nucleation immediately occurs when the incoming solutions initiates supersaturation. With appropriate pH value and suitable concentration of chelating agent, the nucleation rate can be controlled and the formed crystal nucleuses grow to single crystalline grains gradually. Second, the single crystals agglomerate together to form polycrystalline crystallites, known as primary particles of precursors. Then the primary particles further cluster to form embryonic agglomerates (**Figure 1**a). Third, spherical secondary particles form, grow, and consolidate by agglomeration of embryonic agglomerates, growth of primary particles in the agglomerates and adhering of newly formed primary particles, accompanied with recrystallization (Figure 1b). The consolidation and surface smoothing can be explained by the dissolution and recrystallization phenomena (Figure 1c), which are driven by the surface free energy and can be described by the Kelvin equation (Equation (3))[20]

$$\ln\left(S/S_0\right) = \left(2\sigma/p_L\right)\left(M/\rho RT\right) \tag{3}$$

where S and S_0 are the solubility of crystals on curved surface and planar surface, respectively, σ is the solid/liquid surface tension, p_L is the curvature radius of crystal surface, M is the molecular weight of the crystal, ρ is the density of the crystal, R is the universal gas constant, and T is the absolute temperature. If the curvature of the crystal surface is convex, the p_L is positive, and then S is larger than S_0. This means the sharp edges of the crystals, which are convex, are easy to redissolve. In contrast, at the junctions of contacted crystals, the surfaces are concave ($p_L < 0$), and have lower solubility than the planar surfaces. Hence, the concave surfaces are ideal sites for recrystallization. Driven by this mechanism, the formed secondary particles become denser and smoother.

As Ni-rich cathode materials can inherit physical features from their precursors, controlling the particle growth, including the primary particles and the secondary particles, is of great importance to producing ideal precursors that can endow the cathode materials with excellent electrochemical properties.

3.1. Growth Control of Primary Particles

Diffusion properties of Li+ ions in Ni-rich layered cathode materials are largely determined by the crystallographic structure of their primary particles, which are formed during the synthesis and driven by thermodynamics. Interestingly, they are related to the microstructures of the primary particles of the precursors. In a typical layered structure (R-$3m$ space group), as shown in **Figure 2**a, TMO_6 octahedrons are connected with each other to form planes which are perpendicular to c-axis, and indexed as {001} facets; Li+ ions occupy the octahedral voids between adjacent oxygen layers.[21] The {001} facets do not provide diffusion paths for Li+ ions, so they are electrochemically inert. The {010} facets, which are parallel to c-axis, allow Li insertion and extraction along a-axis and b-axis. These facets include (010) plane, (0-10) plane, (100) plane, (-100) plane, (110) plane, and (1-10) plane. The diffusion paths for Li+ ions are schematically illustrated in Figure 2b. From this point of view, exposing more {010} facets can facilitate Li transportation, thus enabling high rate capability.[22] Although the crystallographic structure of a
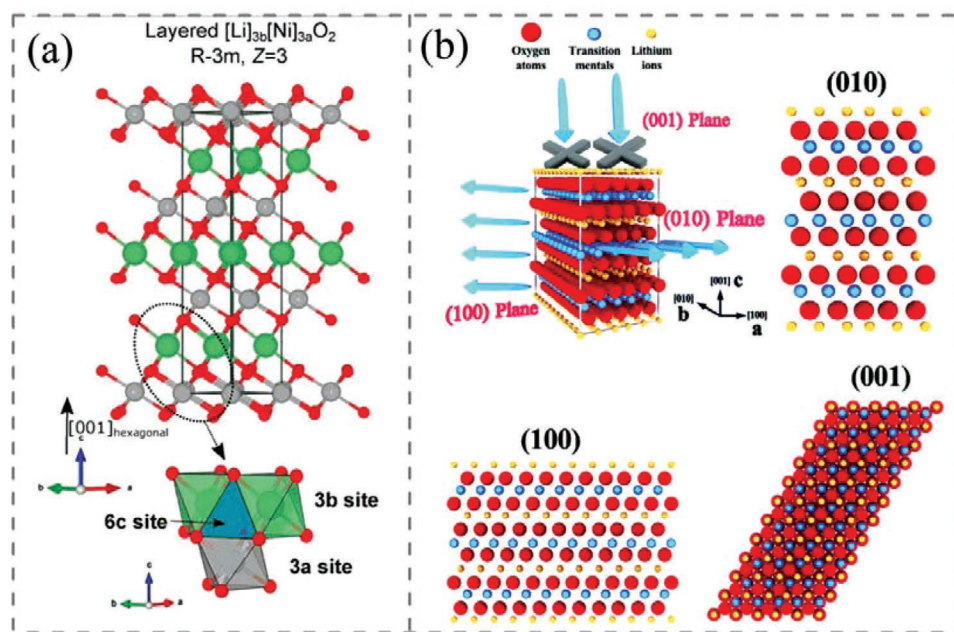
Figure 2. a) Crystallographic structure of layered $LiNiO_2$. Reproduced with permission.[21] Copyright 2019, John Wiley and Sons. b) Schematic illustration of diffusion paths for Li ions, together with the (010) plane, (100) plane, and (001) plane of layered cathode materials. Reproduced with permission.[22a] Copyright 2018, The Royal Society of Chemistry.

layered cathode is formed during high-temperature synthesis, the proportion of the electrochemically active facets can be regulated by controlling crystal growth of precursors.

In a coprecipitation process, the growth of primary particles is usually in an anisotropic mode, even with vigorous stirring. This is ascribed to the difference in the surface energy of their surfaces. Calculation based on density functional theory (DFT) for $Ni_{1/3}Co_{1/3}Mn_{1/3}(OH)_2$ precursor, conducted by Yang et al.,[20] revealed that (001) planes possessed the highest surface energy that led to the highest growth rate along [001] direction, as shown in Figure 3a. Besides, the electronegativity varies from one surface to another, resulting in the growing along certain preferred orientations, because the electronegativity of a certain surface affects its adsorption behavior to other ions or molecules. **Figure 3**a illustrates that the concentration of hydroxyl on (001) plane is the highest. This is the reason why (001) plane has strong affinity to positively charged ions or groups. Therefore, in order to produce a precursor with desirable properties, anisotropic growth of primary crystals can be controlled by regulating the surface characteristics. For example, Fu et al.[23] employed a poly(vinylpyrrolidone) (PVP)-assisted coprecipitation to synthesize a hexagonal flake-like $Ni_{1/3}Co_{1/3}Mn_{1/3}(OH)_2$ precursor (Figure 3b). The PVP acted as a surface-capping agent which adsorbed on the negatively charged {001} surfaces via their amine groups, consequently hindering the growth along [001] direction. Under this condition, ultra-thin $Ni_{1/3}Co_{1/3}Mn_{1/3}(OH)_2$ nanoflakes with high area of {001} facets were obtained. These ultrathin nanoflakes could aggregate along [001] direction to form thick plate-like cathode particles under an appropriate lithiation temperature. When calcined with LiOH at 900 °C, single crystalline $LiNi_{1/3}Co_{1/3}Mn_{1/3}O_2$ with a hexagonal plate-like morphology and high percentage of exposed {010} facets could be obtained

(Figure 3c). At a high current density of 15 C (1 C = 160 mA g^{-1}), the cathode still exhibited a discharge capacity of 130 mAh g^{-1} (Figure 3d,e). In addition, concentration of dissociative ammonia also has significant effect on the crystal growth, since ammonium ions tend to adsorb on electronegative crystal planes. Yang et al.[10a] synthesized a series of $Ni_{0.815}Co_{0.15}Al_{0.035}(OH)_2$ precursors with various concentrations of ammonia as chelating agent. They found that the epitaxial growth of (101) plane was preferential when the concentration of NH_4OH was lower than 1.5 mol L^{-1} (Figure 3f,g). The cathode synthesized from the (101) plane-dominated precursor showed better rate capability (Figure 3j). When the concentration was higher than 2.0 mol L^{-1}, the growth of (001) plane turned to overwhelming dominance (Figure 3h,i), which engendered inferior rate capability but better cycling stability (Figure 3j,k).

The size and arrangement of primary particles in precursors also have significant influence on the electrochemical performance of the targeted cathode materials. The size of primary particles can be controlled by the supersaturation in the solution.[24] High supersaturation in a solution with high pH value facilitates nucleation, thereby suppressing the particle growth.[25] Duan et al.[26] synthesized a series of $Ni_{0.8}Co_{0.15}Al_{0.05}(OH)_2$ precursors at various pH values. The result showed that the size of primary particles became smaller with higher pH value (**Figure 4**a–d). However, their results showed that the cathode material did not inherit the particle size of the precursor. On the contrary, larger cathode crystals were obtained from the precursor with smaller primary particles (Figure 4e–h). The reason for this phenomenon is that smaller particles possess higher specific surface area and more easily fuse together to form lager crystals with good crystallinity during high-temperature calcination. Hence, smaller primary particles in precursor are more suitable for the synthesis of single-crystal cathode
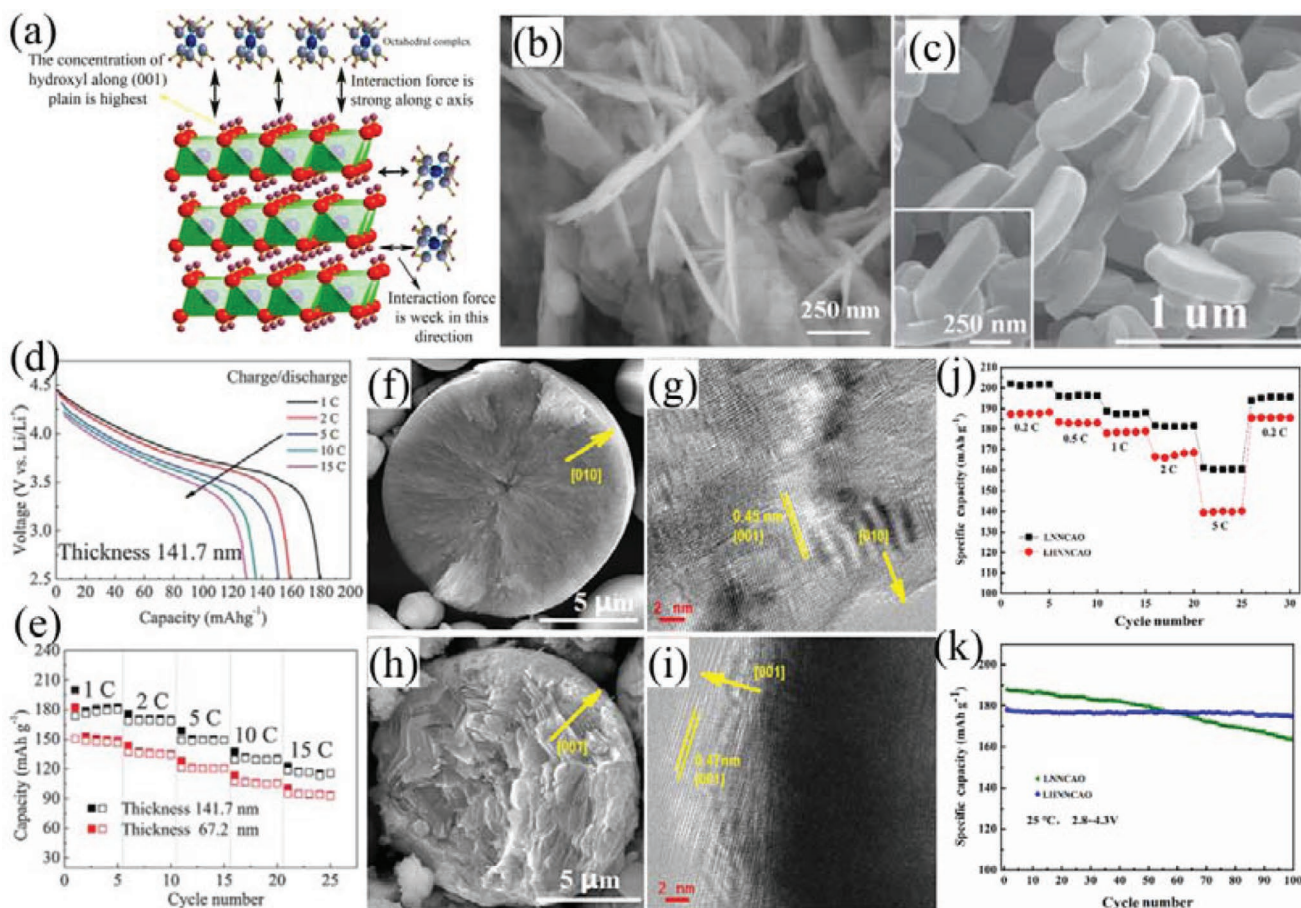
ADVANCED
SCIENCE NEWS
www.advancedsciencenews.com

NANO · MICRO
small
www.small-journal.com

Figure 3. a) Mechanism of anisotropic growth of $Ni_{1/3}Co_{1/3}Mn_{1/3}(OH)_2$. Reproduced with permission.[20] Copyright 2015, Elsevier. Scanning electron microscopy (SEM) images of b) thin flake-like $Ni_{1/3}Co_{1/3}Mn_{1/3}(OH)_2$ precursor synthesized by PVP-assistant coprecipitation and c) the corresponding $LiNi_{1/3}Co_{1/3}Mn_{1/3}O_2$, together with d) discharge curves at various current densities and e) rate capabilities of the corresponding cathodes with different thickness. Reproduced with permission. [23] Copyright 2013, The Royal Society of Chemistry. SEM and high-resolution transition microscopy (HRTEM) images of $Ni_{0.815}Co_{0.15}Al_{0.035}(OH)_2$ precursors synthesized with ammonia concentration of f,g) 0.5 mol L^{-1} and h,i) 2 mol L^{-1}, together with j) rate capabilities and k) cycling performances of the corresponding cathodes (LNNCAO: synthesized from the precursor obtained at an ammonia concentration of 0.5 mol L^{-1}; LHNNCAO: synthesized from the precursor obtained at an ammonia concentration of 2 mol L^{-1}). Reproduced with permission.[10a] Copyright 2021, Elsevier.

materials, which usually possess improved cycling stability due to the crack-resistance characteristics, low specific area and good crystallinity.[8b,27] This has also been demonstrated by the comparison of cycling performances between the single-crystal $LiNi_{0.8}Co_{0.15}Al_{0.05}O_2$ (NCA3 in Figure 4i) synthesized from the precursor with smaller primary particles (Figure 4d) and commercial polycrystalline counterpart (SNCA in Figure 4i). However, the authors found that the single-crystal cathode had inferior rate capability to the polycrystalline one, resulting from the longer paths for Li+ diffusion (Figure 4j).

For controlling the arrangement of primary particles, Yang et al.[10b] simultaneously controlled the pH value and ammonia concentration in their experiment to synthesize $Ni_{0.6}Co_{0.2}Mn_{0.2}(OH)_2$ precursors with different arrangement of primary particles. They found that at lower pH value and higher ammonia concentration, the decreased nucleation and increased complexation facilitated the formation of closely packed plate-like primary particles, whereas higher pH value and lower ammonia concentration caused smaller and

disorderly packed ones, as shown in **Figure 5**a–d. The distinct arrangements of primary particles could be inherited by the cathode materials, as shown in Figure 5e–g. The primary particles laid in an ordered radial direction provided unobstructed channels for Li+ diffusion, therefore leading to higher specific capacity and better rate capability (Figure 5h,i). The merits of the orderly arranged primary particles in the cathode material is illustrated in Figure 5j–l.

Endowing cathode materials with desired electrochemical properties by inheriting morphological features from precursors also deserves exploration in other cathode materials. Wu et al.[28] fabricated flake-like $Co(OH)_2$ precursor using a simple coprecipitation method. In their work, $CoSO_4·7H_2O$ and $(NH_4)_2SO_4$ were dissolved to form a solution, and then dropped into NaOH solution. In this process, thin $Co(OH)_2$ flakes could be obtained without adding any surfactant. Being similar to the results reported by Fu et al.[23], the thin flake-like precursor was made into thick $LiCoO_2$ flakes with high percentage of {010} facets, which delivered a discharge capacity of 96 mAh g^{-1} at
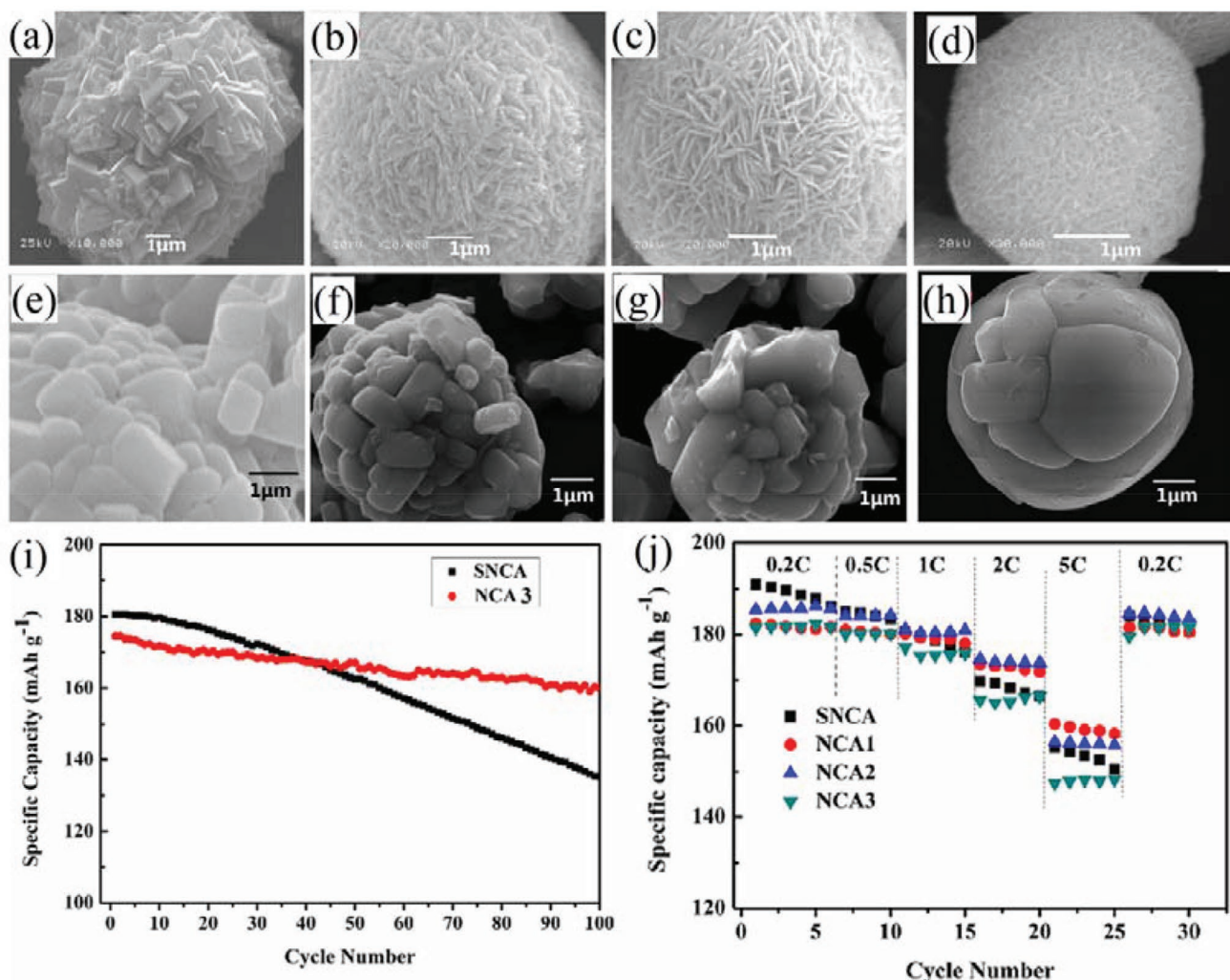
ADVANCED
SCIENCE NEWS
www.advancedsciencenews.com

NANO · MICRO
small
www.small-journal.com

Figure 4. a–d) SEM images of $Ni_{0.8}Co_{0.15}Al_{0.05}(OH)_2$ precursors prepared at pH values of 11.00, 11.25, 11.50, and 12.00, respectively, and e–h) SEM images of $LiNi_{0.8}Co_{0.15}Al_{0.05}O_2$ synthesized from the precursors shown in (a–d); comparison of i) cycling performances and j) rate capabilities between single-crystal $LiNi_{0.8}Co_{0.15}Al_{0.05}O_2$ and commercial spherical counterpart. Reproduced with permission.[26] Copyright 2016, Elsevier.

10 C (1 C = 140 mA g^{-1}). By comparison, the other $LiCoO_2$ sample synthesized using commercial Co_2O_3 as precursor had an octahedron-like morphology, which showed almost no capacity at 10 C.

3.2. Growth Control of Secondary Particles

The microstructural and morphological features of secondary particles of cathode materials are closely related to their tap density and processability. Dense and uniform-sized secondary particles of a cathode material guarantee the energy density of a battery cell, since they can be closely packed on the current collector. Moreover, uniform-sized spherical morphology allows good fluidity that makes the material powder homogeneously disperses in the electrode slurry. It has been demonstrated that the tap density, morphology, and size distribution of cathode materials are determined by their precursors, which in turn, determined by the process parameters in coprecip

itation.[17a,29] Hence, it is necessary to establish a systematical guidance for the precursor developers based on the fundamentals of coprecipitation.

The agglomeration of primary particles will not occur until the primary particles grow to a certain size, because the surfaces of fine primary crystallites become charged in a basic solution. The electrostatic repulsion induced by the charged surfaces hinders the primary particles from agglomeration.[30] With the increase in the size of primary particles, the effect of the repulsion among primary particles is weakened gradually. When the size of the primary particles increases beyond the agglomeration threshold, the propensity to aggregate become consideration and the formation of secondary particles gets started.[31] In the meanwhile, van der Waals force and turbulent agglomeration also increase, which can facilitate the agglomeration of primary particles.[32]

As illustrated by Figure 1b, the growth of secondary particles starts with the agglomeration of primary particles to form embryonic agglomerates. Then, embryonic agglomerates further
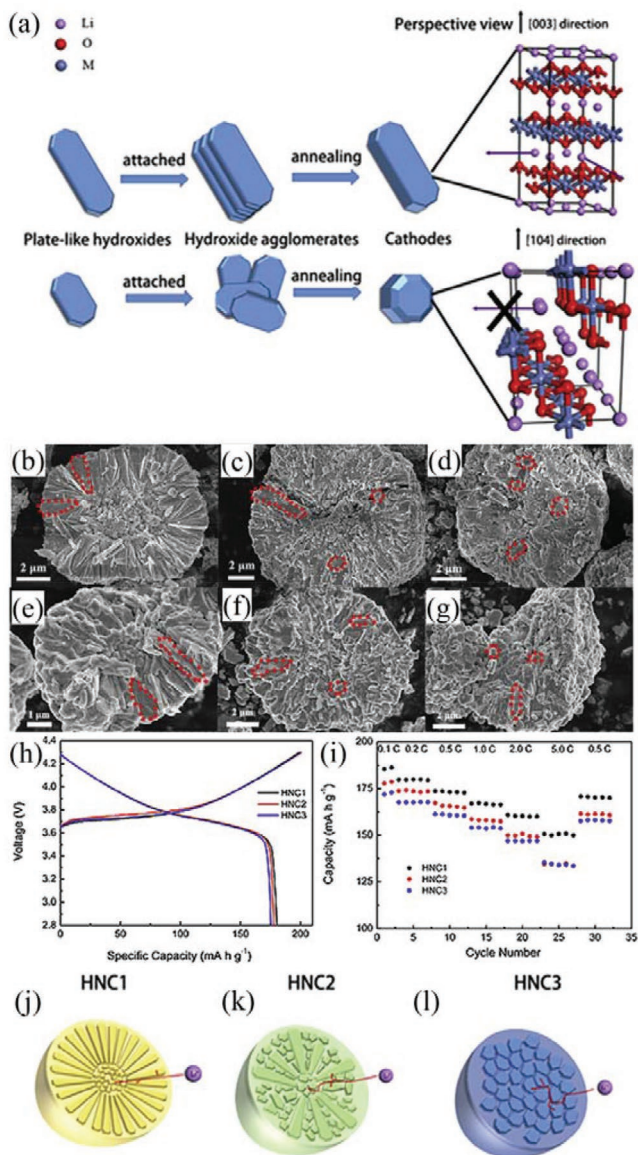
2107697 (6 of 18)

**ADVANCED
SCIENCE NEWS**
www.advancedsciencenews.com

NANO · MICRO
small
www.small-journal.com

Figure 5. a) Schematic illustration of ordered and disordered $Ni_{0.6}Co_{0.2}Mn_{0.2}(OH)_2$ primary particles and the microstructures of their surfaces; cross-sectional SEM images of b–d) the $Ni_{0.6}Co_{0.2}Mn_{0.2}(OH)_2$ precursors and e–g) $LiNi_{0.6}Co_{0.2}Mn_{0.2}O_2$ cathodes with different arrangements of primary particles; comparison of h) typical charge-discharge curves at 0.1 C and i) rate capability between the $LiNi_{0.6}Co_{0.2}Mn_{0.2}O_2$ with different arrangements of primary particles; j–l) schematic illustration of the distinct inner structures. Reproduced with permission.[10b] Copyright 2016, Elsevier.

agglomerate to form embryonic secondary particles. This stage lasts from tens of minutes to several hours. The embryonic secondary particles subsequently undergo growth, spheroidization, consolidation, and smoothing to form mature secondary particles. This stage lasts from tens of hours to more than one hundred hours, and is mainly controlled by the dynamic equilibrium between coprecipitation and dissolution described by Equation (2). In a coprecipitation process, therefore, the growth of secondary particles is affected by the factors related to reactions in solution, including pH value,[17a,30] the concentration of ammonia,[10a] reaction time,[33] agitation velocity,[34] and the concentration of reactants.[35]

In General, the formation of dense and uniform-sized secondary particles requires a slow enough coprecipitation and the occurrence of dissolution-recrystallization in the presence of ammonia, as described by Equations (1) and (2).[19,36] Because the solubility product (K_{sp}) of TM hydroxides is very low (10^{-13}–10^{-15}), such a dissolution-recrystallization mechanism can only occur at a specific pH value range, which can be calculated via the equilibrium constants involved in the coprecipitation, including the equilibrium constants for coordination of ammonia to TM cations, the dissociation constant of aqueous ammonia, the water dissociation constant and the K_{sp} of TM hydroxides.[36a] It has been demonstrated that with a high pH value at which TM cations are more inclined to precipitate with dissociative hydroxyl anions (OH^-) rather than coordination to ammonia, the growth of secondary particles is prevented.[17c,37] A typical comparison among $Ni_{0.5}Co_{0.2}Mn_{0.3}(OH)_2$ precursors synthesized by Noh and Cho[37c] at various pH values and a fixed ammonia/$TMSO_4$ ratio of 0.8 is shown in **Figure 6**a–c. Their experimental result was well consistent with the calculation reported by Barai et al.[30] (Figure 6d,e). The impact of pH value on the growth of secondary particles is originated from the competition between complexation and precipitation, which can also be predicted by calculating the residual concentrations of $[TM(NH_3)_n]^{2+}$ and OH^- in the solution.[19] As can be seen in Figure 6f,g, higher ratio of $[TM(NH_3)_n]^{2+}$ to OH^- indicates that the complexation is more dominant, whereas a lower ratio suggests greater inclination to precipitate. In other words, higher pH value causes larger supersaturation, thus leading to enhanced number density of the nuclei and suppressed particle growth. It is noteworthy that the required pH range at which dense and spherical secondary particles can grow varies for the precursors with different Ni/Co/Mn ratios since the pH range at which the coordination to ammonia occurs is different for different TM cations, as shown in Figure 6h.[36a] Therefore, it is recommended to adjust pH value in case of switching precursor production from one formula to another. In addition, the dissolution-recrystallization mechanism also suggests that for the synthesis of precursors containing the metal cations that have an extremely low K_{sp} in basic solution or do not coordinate with ammonia (such as Al^{3+} in Ni-Co-Al hydroxide precursor), other chelating agents are required for the special cations.[38] Otherwise, rapid precipitation will occur, resulting in the generation of too many nuclei and continuous formation of small particles, as opposed to the growth of secondary particles.

With a fixed pH value, the concentration of ammonia not only has significant impact on the morphology of primary particles (Figure 3f–i), but also affects the growth of secondary particles, since it directly impacts the dynamic equilibrium between coprecipitation and dissolution. Computational prediction conducted by Barai et al.[30] concluded that with a fixed pH value, higher ammonia concentration facilitated the growth of secondary particles by increasing the diffusivity of primary particles. In this case, the secondary particles also keep changing in size throughout the coprecipitation due to agglomeration between adjacent secondary particles, resulting in broadened size distribution and lower tap density. The computational prediction can be supported by some experimental results.[17a,c,37c]
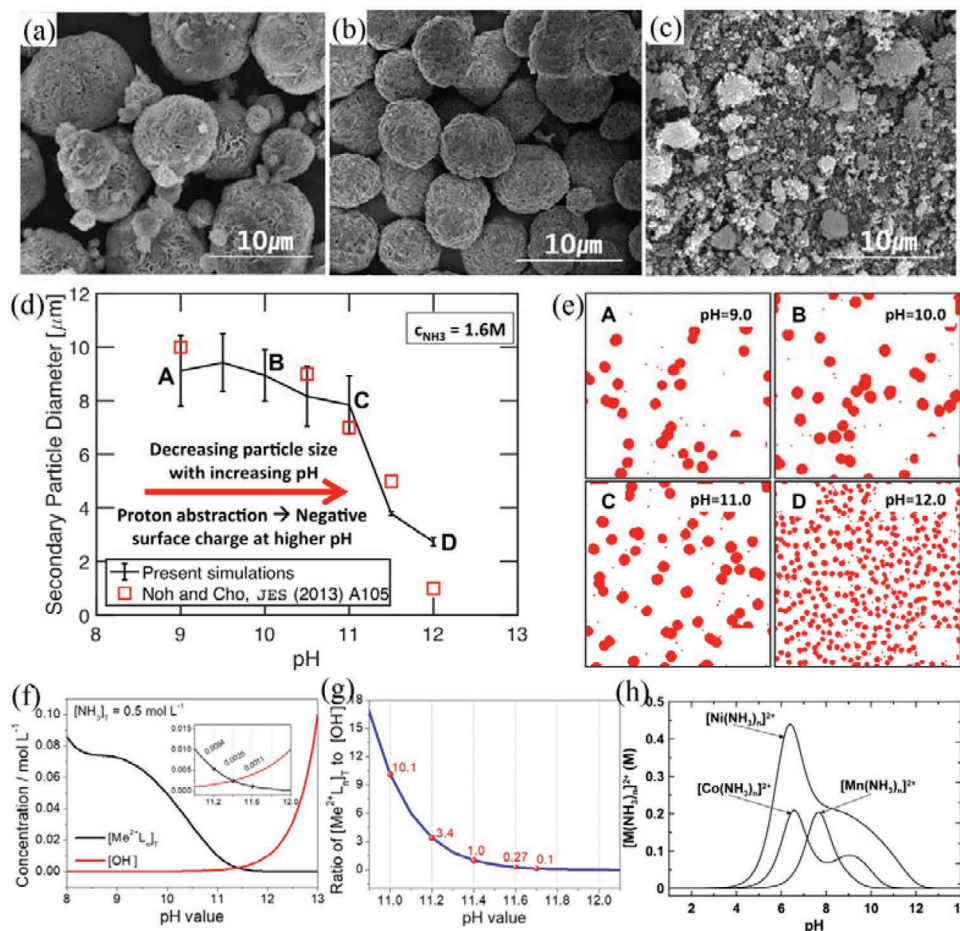
Figure 6. a–c) SEM images of $Ni_{0.5}Co_{0.2}Mn_{0.3}(OH)_2$ precursors synthesized at pH values of 9.0, 11.0, and 12.0, respectively. Reproduced with permission.[37c] Copyright 2013, The Electrochemical Society. d) Experimental result (red squares) and calculated result (black line with error bars) of variations in secondary particle size at various pH values, together with e) the predicted particle size distribution at the corresponding pH values. Reproduced with permission.[30] Copyright 2019, American Chemical Society. f) Calculated residual concentrations of $[TM(NH_3)_n]^{2+}$ (labeled as $[Me^{2+}L_n]_T$ in the figure) and OH^- as a function of pH value at an ammonia concentration of 0.5 M, together with g) the corresponding ratio of $[TM(NH_3)_n]^{2+}$ to OH^-. Reproduced with permission.[19] Copyright 2021, American Chemical Society. h) Effect of pH value on the concentration of $[Ni(NH_3)_n]^{2+}$, $[Mn(NH_3)_n]^{2+}$, and $[Co(NH_3)_n]^{2+}$ (the curve is the sum of the concentrations for complexes with $1 \leq n \leq 6$). Reproduced with permission.[36a] Copyright 2009, American Chemical Society.

Hence, in order to avoid irregular-shaped morphology and broadened size distribution, the ammonia concentration should be optimized at a fixed pH value.

Agitation is another important factor on the growth of secondary particles, since it is responsible for providing favorable conditions for the coprecipitation reaction. First of all, injected TM cations can easily encounter ammonia and hydroxyl anions in an agitated solution. This is a prerequisite for co-precipitation. Second, the growth of dense and spherical particles requires fierce collision among individual crystallites and embryonic agglomerates. This can be induced by vigorous agitation.[39] Third, the fluid motion in a stirred suspension generates fluid shear force that can break weakly-bound agglomerates. In this case, strongly enough binding force can be established within the agglomerated crystallites to resist the fluid shear, thus enabling the formation of dense secondary particles with good integrity and high mechanical strength.[40] It has been demonstrated that agitation speed puts significant impact on the

morphology of hydroxide precursors.[34,37b,c] For example, in Noh et al.'s work, the $Ni_{0.5}Co_{0.2}Mn_{0.3}(OH)_2$ precursor prepared with stirring speed of 300 rpm showed irregular particle shapes and a tap density of 1.08 g cm^{-3}, whereas the sample obtained at stirring speed of 1000 rpm had denser and spherical morphology with a much improved tap density (2.20 g cm^{-3}), as shown in **Figure 7**a,b.[37c] In general, too weak agitation cannot provide stable reaction conditions for mass transfer and enough hydrodynamic fluid shear for the formation of dense particles, while too vigorous agitation makes the coprecipitation less controllable due to the increased randomness of the fluid motion.[34]

In addition to agitation speed, interestingly, the type of impeller used for stirring also shows influence on the particle growth in coprecipitation. Zhu et al.[41] demonstrated that the $Ni_{0.6}Co_{0.2}Mn_{0.2}(OH)_2$ precursor synthesized with a propeller turbine (PT) (Figure 7e) had higher density and smoother surface (Figure 7d) than the one synthesized with a Rushton turbine (RT) (Figure 7g,h). In fact, the essence behind the effect of

**ADVANCED
SCIENCE NEWS**

www.advancedsciencenews.com

NANO · MICRO

small

www.small-journal.com

agitation on the particle growth is the fluid motion. An ideal fluid motion should provide steady and fast mass transfer and appropriate fluid shear. Figure 7c shows a typical Taylor vortex flow, an axially periodic fluid motion induced in the gap between two coaxial cylinders with rotating inner cylinder and stationary outer one, which can promote mass transfer.[42] Figure 7f,i shows the difference between the flow fields generated by the PT and RT impellers. With the axial flow generated by a PT impeller, the feed-in TM cations can be quickly transported to the bulk of the suspension, and the supersaturation is small throughout the whole reactor (Figure 7f). With the RT impeller, however, the fluid motion is radial-dominated and segregated into two loops (Figure 7i), leading to retarded mass transfer between the upper and lower loops.[43] This makes the mass distribution in the reactor inhomogeneous. The cathode made from the dense precursor shows higher capacity and much improved cycling stability (shown in Figure 7j,k) Hence, in order to obtain dense and spherical secondary particles, more attentions should be paid on the fluid motion, which involves agitation speed, impeller shape, and the interior construction of the employed reactor.

It is worth mentioning that the growth speed of secondary particles is not uniform during the coprecipitation. At the beginning, the growth of secondary particles is mainly originated from the agglomerate of primary crystallites and exhibits a high growth speed. Subsequently, the effect of the dynamic equilibrium between coprecipitation and dissolution described by Equation (2), as well as Ostwald ripening, becomes prominent.[30] As a result, the growth speed is gradually slowed down; instead, the secondary particles become more spherical, denser and smoother. In general, dense and spherical particles can be obtained after 10–20 h.[17a,20,36a] Kim et al.[33] investigated the growth kinetics of $Ni_{0.855}Co_{0.145}(OH)_2$ particles in continuous coprecipitation process. They figured out the relationship of growth rate and feeding rate, which could be used to direct the reaction time in coprecipitations.

4. Precursor Modifications by Coprecipitation

Ni-rich layered cathode materials have some intrinsic shortcomings, such as unsatisfactory structural stability and surficial stability. To date, great efforts have been devoted to the modifications for them. Considering that commercial Ni-rich cathode materials are synthesized from spherical precursors commonly with a diameter of ≈10 μm, sometimes applying modifications to precursors instead of cathode materials will be more effective. For instance, bulk doping should be implemented during the coprecipitation synthesis of precursors; otherwise, the doping elements can hardly homogeneously permeate throughout such 10 μm scale particles via solid-state calcination. In addition, some modification strategies such as preoxidation,[44] surface modification,[45] core–shell construction,[46] and concentration-gradient[47] have been well-established.

4.1. Preoxidation

Li^+/Ni^{2+} cation mixing in Li slabs, which mainly results from the calcination conditions, is a non-negligible problem for Ni-rich

layered materials.[45a,48] As the Ni^{3+} ions in the layered cathodes are relatively unstable, the presence of Ni^{2+} ions, which have similar ionic radius to Li^+ and readily migrate to Li slabs, cannot be completely prevented during the calcination.[48b] Hence, optimizing the calcination conditions is a primary means to decrease the cation mixing.[48c] Interestingly, preoxidation of precursor can be an indirect way to suppress the cation mixing, since it can effectively enhance the average oxidation state of Ni for the targeted cathode materials. Zhang et al.[44b] utilized $Mn(NO_3)_2$ to preoxidize $Ni_{0.8}Co_{0.1}Mn_{0.1}(OH)_2$ precursor, and the obtained $LiNi_{0.8}Co_{0.1}Mn_{0.1}O_2$ cathode showed suppressed cation mixing and improved cycling stability. Zhou et al.[44c] preoxidized $Ni_{0.8}Co_{0.1}Mn_{0.1}(OH)_2$ precursor using a 30% H_2O_2 solution. The preoxidized precursor could be calcined under CO_2-free air atmosphere to form $LiNi_{0.8}Co_{0.1}Mn_{0.1}O_2$ cathode material, which exhibited improved rate capability and cycling stability. Zhang et al.[49] utilized $Na_2S_2O_8$ solution to preoxidize $Ni_{0.8}Co_{0.1}Mn_{0.1}(OH)_2$ precursor for 30 min, and then synthesized $LiNi_{0.8}Co_{0.1}Mn_{0.1}O_2$ cathode material. The preoxidation endowed the cathode material with well-ordered surface structure and decreased cation mixing, which guaranteed remarkably improved rate capability and cycling performance.

The aforementioned preoxidation treatments are implemented on ready-made precursors. It has been demonstrated that preoxidation can also be carried out during the coprecipitation process. For example, Cheng et al.[44a] synthesized preoxidized $Ni_{0.65}Co_{0.15}Mn_{0.20}(OH)_2$ precursors by controlling the oxygen concentration in the coprecipitation process. In their work, with the increase of oxygen introduced in the coprecipitation, the primary particles became smaller and the specific surficial area became larger (**Figure 8**a–d), consequently promoting the growth of single-crystal cathode material with good crystallinity in the successive calcination (Figure 8e–h). The reason for this phenomenon is that oxygen in the coprecipitation process can lead to increased nucleation of MnO_2 in the solution. Figure 8i schematically illustrates the effect of preoxidation on the precursor morphology and the size of the obtained single-crystal cathode material. In addition, the preoxidation in Cheng et al.'s work decreased the Li^+/Ni^{2+} mixing. As a result, the $LiNi_{0.65}Co_{0.15}Mn_{0.20}O_2$ cathode synthesized from the preoxidized precursor showed improved cycling stability, as shown in Figure 8j.

4.2. Bulk Doping

Bulk-doping is an effective strategy for stabilizing the crystal structures of Ni-rich cathode materials.[50] It has been demonstrated that many TM cations (e.g., Mn^{3+}, Cr^{3+}, Co^{3+}, Fe^{3+}, Zr^{4+}, Ti^{4+}, W^{6+}, etc.) and main group cations (e.g., Mg^{2+}, Al^{3+}, Ga^{3+}, etc.) as dopants have positive effects on the electrochemical performance for Ni-rich cathode materials.[51] The processes adopted to incorporate dopants into the structures of cathode materials can be divided into two categories. For one thing, dopants can be incorporated into the targeted cathode materials during the high-temperature lithiation after mixing the dopants and lithium source with the undoped precursors (solid-state doping).[52] For another, dopants can be added to the coprecipitation solutions so that element-doped precursors can be obtained.[7a,53] In general,
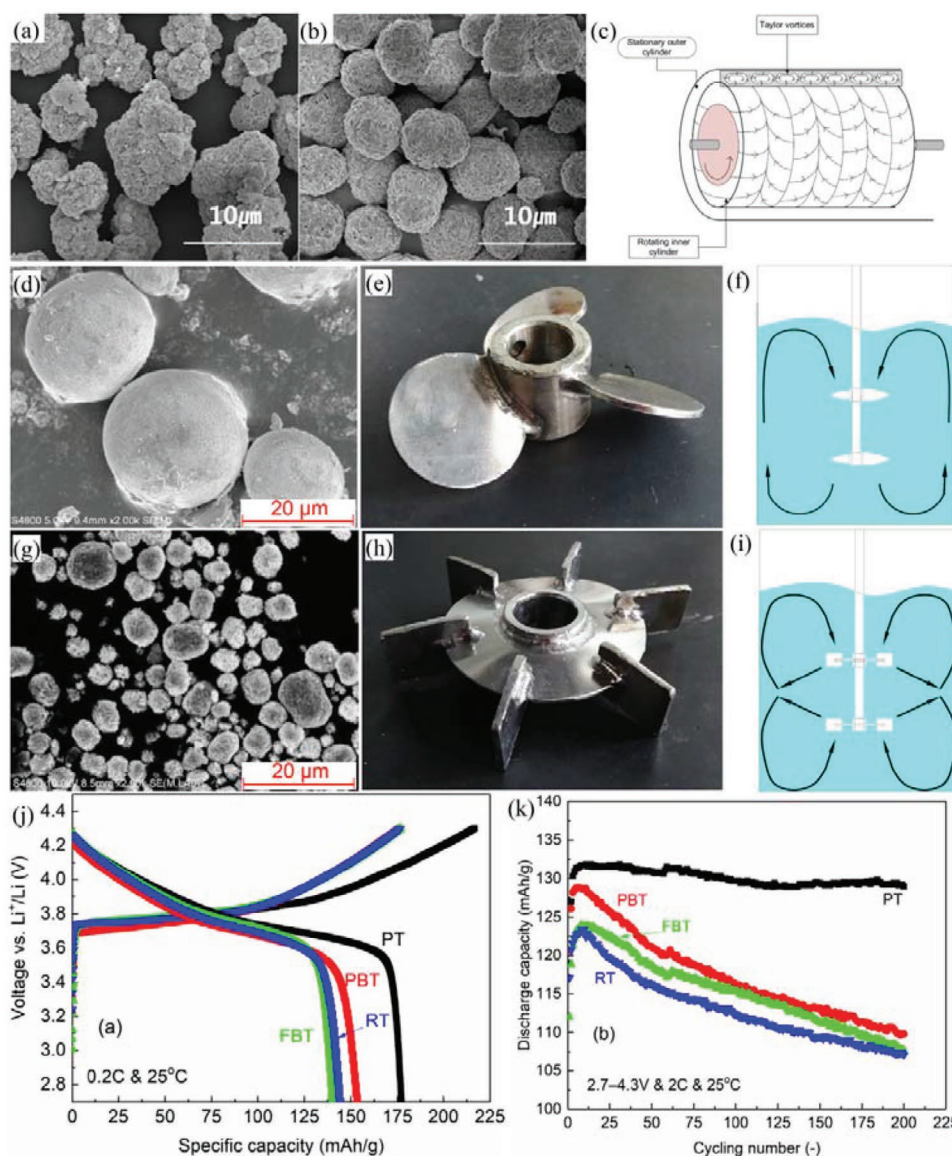
**ADVANCED
SCIENCE NEWS**

www.advancedsciencenews.com

**NANO · MICRO
small**

www.small-journal.com

Figure 7. a,b) SEM images of $Ni_{0.5}Co_{0.2}Mn_{0.3}(OH)_2$ precursors synthesized at agitation speeds of 300 and 1000 rpm, respectively. Reproduced with permission.[37c] Copyright 2013, The Electrochemical Society. c) Schematic diagram of Taylor vortices in a Couette–Taylor reactor. Reproduced with permission.[40] Copyright 2015, Elsevier. d,g) SEM images of $Ni_{0.6}Co_{0.2}Mn_{0.2}(OH)_2$ precursors synthesized with e) propeller turbine (PT) and h) Rushton turbine (RT), respectively; f,i) the flow fields generated by the two impellers; j) initial charge–discharge curves and k) cycling performances of the cathodes synthesized from the precursors obtained with different impellers. Reproduced with permission.[41] Copyright 2019, Elsevier.

the former method cannot guarantee a homogeneous distribution of dopants in the cathode structures due to the slow mass transfer during solid-state annealing. Instead, surface-doping or concentration-gradient doping could be more possible.[54] Also, to the best of our knowledge, detailed characterizations focusing on the coordination of dopants in the targeted cathode materials are rare and difficult, especially for small amounts of dopants. Hence, more attention should be paid to the destination of the dopants, i.e., going into the lattice or staying as segregated phases.

Incorporation of dopants in the structures of precursors by coprecipitation usually achieves more homogeneous distribution of dopants than the solid-state doping. Even so, it should be noted that the dopants might precipitate at different pH values than the precursor, thereby resulting in segregated particles. In addition,

adding dopants during coprecipitation may also affect the morphology of precursor particles. Based on the particle growth mechanism described by Equations (1) and (2), dense and spherical particles require slow nucleation rate. Hence, the dopants that do not chelate with ammonia could not be directly added into the TM solutes used for coprecipitation. Otherwise, rapid nucleation and continuous formation of small particles will occur, thus preventing the growth of secondary particles. For example, in the synthesis of $Ni_{1-x-y}Co_xAl_y(OH)_2$ precursors, $NaAlO_2$ solution is usually used as an individual Al source instead of mixed Ni-Co-Al sulfate solution,[38b,55] as shown in **Figure 9**a. With the increase of Al content fed in the coprecipitation system, loose particles with wider size distribution will be obtained, as shown in Figure 9b–d. Moreover, for W-doping, WO_3 dissolved in NaOH solution can
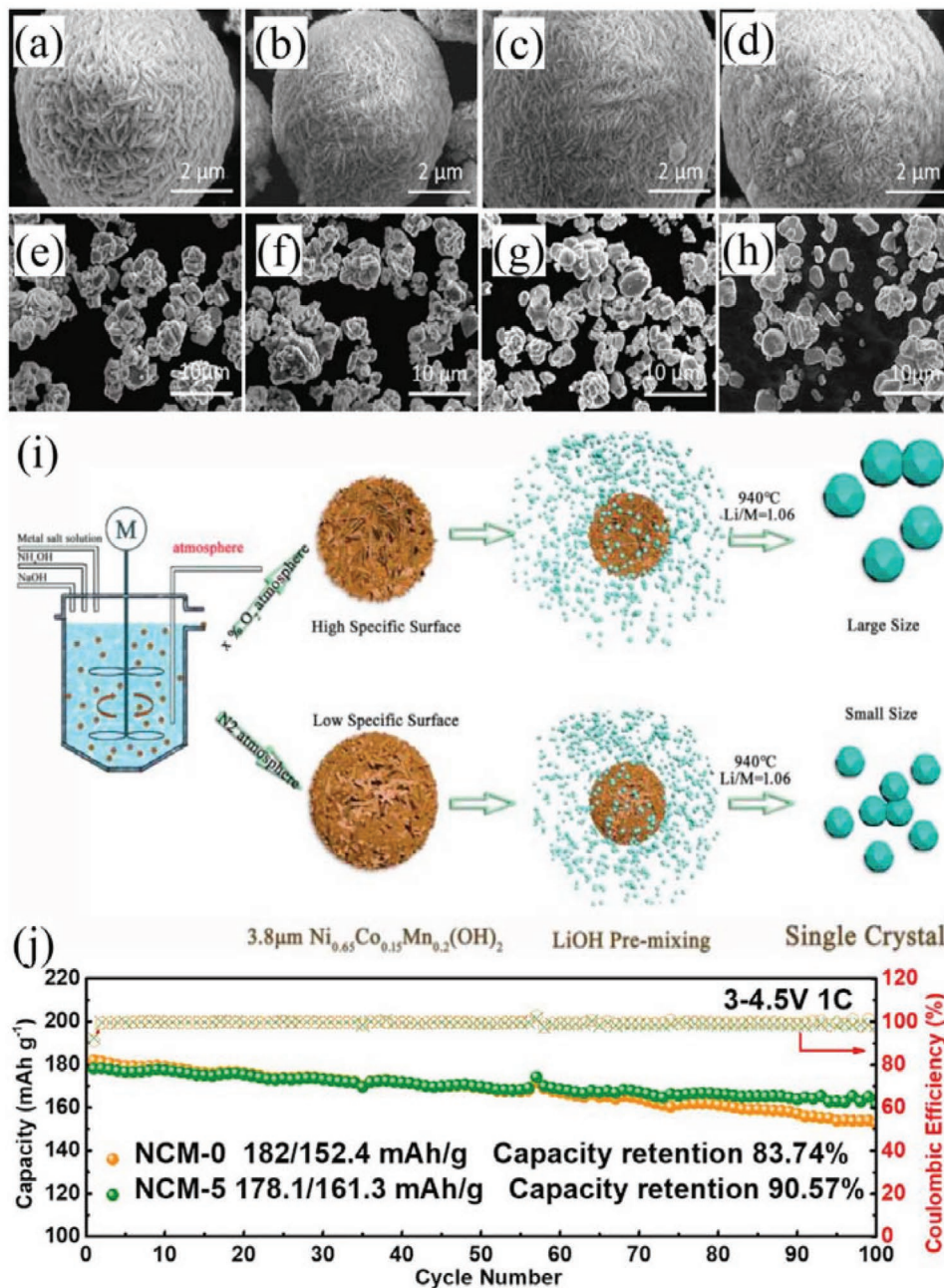
Figure 8. SEM images of a–d) $Ni_{0.65}Co_{0.15}Mn_{0.20}(OH)_2$ precursors synthesized under the atmospheres with various oxygen contents (a: 0%, b: 2.5%, c: 5%, and d: 10%) and e–h) the corresponding $LiNi_{0.65}Co_{0.15}Mn_{0.20}O_2$ cathode materials; i) schematic illustration of the effect of preoxidation on the precursor morphology and the size of the obtained single-crystal cathode material; j) comparison of cycling performances between the pristine sample and the one synthesized from the precursor preoxidized by an atmosphere containing 5% oxygen. Reproduced with permission.[44a] Copyright 2021, from Elsevier.

be used as W source.[7a,53b] The homogeneously dispersed W can effectively suppress the formation of microcracks in the secondary particles (Figure 9e,f), thus improving the electrochemical performance (Figure 9g). Another point deserves further investigations is the effect of dopants on the crystallinity of the cathodes. Although good crystallinity can be easily obtained under common calcination (700–900 °C), dopants might affect the particle growth of precursors, and thereby have impact on the crystallinity of the cathodes during calcination.

4.3. Surface Modification

Surface modification, including surface coating, surface doping, and washing, is a frequently-used strategy to improve the electrochemical performance of layered cathode materials.[56] Surface modifications can be conducted not only on cathode materials, but also on precursors. For the latter, the precursors are usually coated with one or more functional compounds before high-temperature lithiation. A common

ADVANCED
SCIENCE NEWS
www.advancedsciencenews.com

NANO · MICRO
small
www.small-journal.com

phenomenon is that the elements in the coating layer can diffuse into the bulk of the cathode material during the calcination. It should be pointed out that the element diffusion behavior is driven by thermodynamics, which is largely determined by the calcination conditions, especially temperature. Therefore, more attention should be paid to the calcination conditions while conducting surface modifications, as the surface coating and surface doping have different effects on the electrochemical properties on cathode materials.[57] Lee and Park[57d] compared the surface coating on $Ni_{0.82}Co_{0.12}Mn_{0.06}(OH)_2$ precursor with the direct surface coating on $LiNi_{0.82}Co_{0.12}Mn_{0.06}O_2$ cathode, and found that the former technology resulted in better rate capability and cycling performance due to the doping effect of the coating materials. Lee et al.[57a] utilized SiP_2O_7 nanoparticles to coat $Ni_{0.5}Co_{0.2}Mn_{0.3}(OH)_2$ precursor, and then calcined the SiP_2O_7-coated precursor with Li source to synthesize surface-modified $LiNi_{0.5}Co_{0.2}Mn_{0.3}O_2$ cathode material. During the calcination, not only did P and Si penetrate into the cathode material, but also the SiP_2O_7 was converted into amorphous $Li\delta P_yO_z$ coating on the cathode particles. The synergistic effect of the P-/Si-codoping and $Li\delta P_yO_z$-coating endowed the cathode material with improved rate capability and thermal stability.

In addition to the surface-doping effect, calcination of surface-coated precursor can slightly flatten the elements distribution near the interface between coating layers and precursors, resulting in near-surface concentration-gradient cathode materials.[45a,58] Huang et al.[45a] treated $Ni_{0.8}Co_{0.15}Al_{0.05}(OH)_2$ precursor using $KMnO_4$ solution. In their work, MnO_4^- anions were converted into MnO_2 and uniformly precipitated on the surface of the precursor. The MnO_2-coated precursor was then calcined with $LiOH \cdot H_2O$ to form $LiNi_{0.8}Co_{0.15}Al_{0.05}O_2$ cathode material with a Mn-rich surface. The surface-modified cathode showed improved cycling stability and higher tolerance to moisture air. Li et al.[58c] coated $Ni_{0.8}Co_{0.1}Mn_{0.09}Al_{0.01}(OH)_2$ with $La(NO_3)_3 \cdot 6H_2O$ and then synthesized a La-modified $LiNi_{0.8}Co_{0.1}Mn_{0.09}Al_{0.01}O_2$ which had a concentration gradient of La and Ni existed in a limited depth (less than 2 µm) from the surface. Such cathode material with La-rich surface exhibited an improved cycling stability compared with $LiNi_{0.8}Co_{0.1}Mn_{0.09}Al_{0.01}O_2$ and $LiNi_{0.8}Co_{0.1}Mn_{0.1}O_2$.
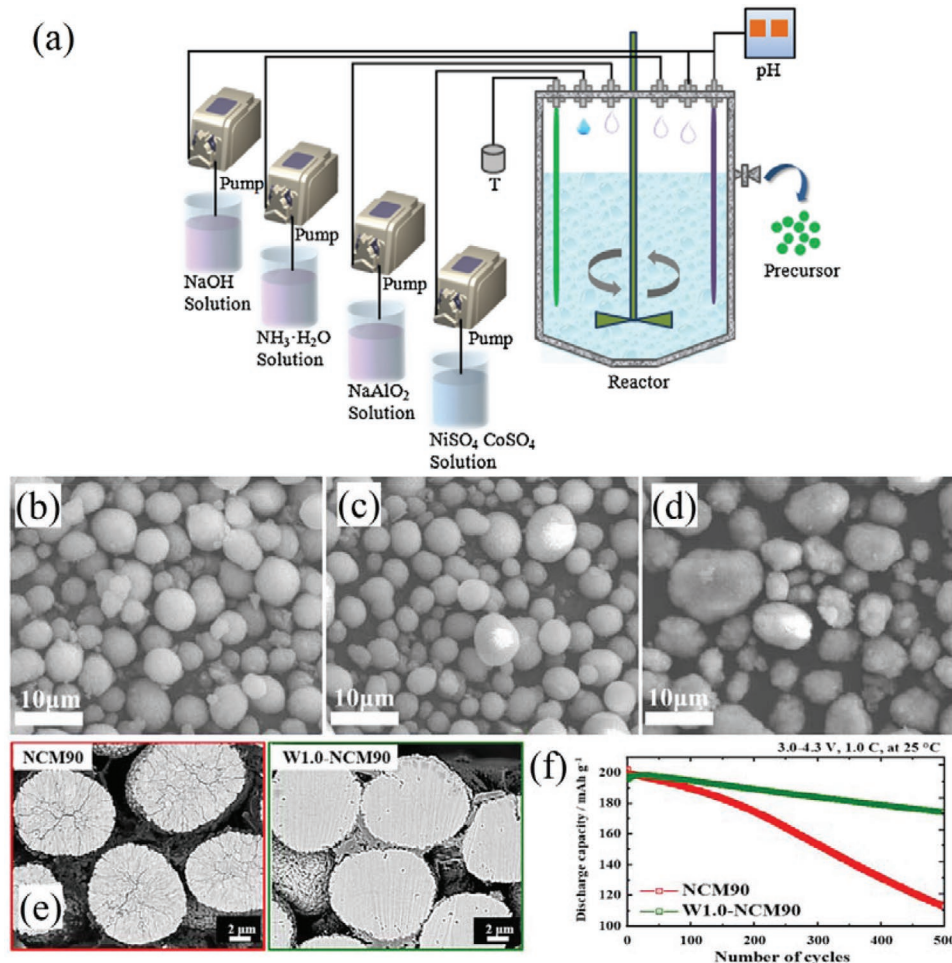

Figure 9. a) Schematic illustration of coprecipitation synthesis of $Ni_{0.85-x}Co_{0.15}Al_xO_2(OH)_2$ precursor; b–d) SEM images of $Ni_{0.83}Co_{0.15}Al_{0.02}(OH)_2$, $Ni_{0.80}Co_{0.15}Al_{0.05}(OH)_2$, and $Ni_{0.75}Co_{0.15}Al_{0.10}(OH)_2$, respectively. Reproduced with permission.[38b] Copyright 2017, Elsevier. e) Cross-sectional SEM images of $LiNi_{0.90}Co_{0.05}Mn_{0.05}O_2$ (NCM90) and 1 at% W-doped NCM90, together with f) the comparison of their cycling performances. Reproduced with permission.[7a] Copyright 2019, Elsevier.

**ADVANCED
SCIENCE NEWS**

www.advancedsciencenews.com

**NANO · MICRO
small**

www.small-journal.com

4.4. Core–Shell Construction and Concentration-Gradient Precursors

Sun et al.[46c] reported a core–shell-structured Li[(Ni$_{0.8}$Co$_{0.1}$Mn$_{0.1}$)$_{0.8}$(Ni$_{0.5}$Mn$_{0.5}$)$_{0.2}$]O$_2$ cathode material synthesized from a [(Ni$_{0.8}$Co$_{0.1}$Mn$_{0.1}$)$_{0.8}$(Ni$_{0.5}$Mn$_{0.5}$)$_{0.2}$](OH)$_2$ precursor which was obtained by coprecipitation (as shown in **Figure 10**a). The precursor was composed of a Ni-rich core [Ni$_{0.8}$Co$_{0.1}$Mn$_{0.1}$(OH)$_2$] and a low-Ni shell [Ni$_{0.5}$Mn$_{0.5}$(OH)$_2$] with a clear boundary between them (Figure 10b). By inheriting the microstructure from the precursor, the core–shell cathode material possessed high specific capacity endowed by the Ni-rich core and satisfactory cycle life resulting from the stable shell. The core–shell-structured cathode showed improved discharge capacity and cycling stability than the LiNi$_{0.8}$Co$_{0.1}$Mn$_{0.1}$O$_2$ cathode (Figure 10c,d). Their strategy initiated a new way to improve electrochemical performance of Ni-rich layered cathode materials. After then many similar works have been published.[46a,b,59] For the synthesis of core–shell-structured precursors, coprecipitation shows excellent facility and controllability, since it can conveniently control the thickness of the shell by regulating the reaction time,[46b] and control the composition of the shell by adjusting the composition of the TM solution used for constructing the shell.[59a-c]

Although a core–shell structure can effectively mitigate some disadvantages of Ni-rich cathode materials, there are still some issues with it. For example, in a core–shell-structured cathode particle, the volume change of the core is usually different from that of the shell due to the difference in their Ni content.[5b] As a result, the shell gradually separates from the core, leading to breakage of diffusion pathway for Li$^+$ ions from the core.[47e] In addition, the manufacture of core–shell-structured precursor can only adopt batch-type process which is inferior to continuous process in productivity and quality consistency.

In order to address the structural mismatch between core and shell in core–shell materials, concentration-gradient materials are explored.[47b-e] Obviously, concentration-gradient precursors must be prepared at first. A typical synthesis of a concentration-gradient precursor can be briefly described as following. First of all, Ni-rich spherical cores are pre-prepared. Then, for the growth of the concentration-gradient outer layer on the Ni-rich core, Ni-poor solution is slowly fed into Ni-rich solution, after which the homogeneously mixed solution is fed into the coprecipitation reactor, as shown in **Figure 11**a. With the continuous mixing of the Ni-poor and Ni-rich solutions, the total Ni concentration in the reactor decreases gradually, leading to a descending concentration of Ni from the inner to the outer for the obtained precursor, as well as the lithiated cathode material (Figure 11b,c). Similar to core–shell materials, concentration-gradient materials possess improved structural and thermal stability. However, the structural mismatch encountered by core–shell materials can be eliminated in concentration-gradient materials. Sun et al.[47b] demonstrated that the concentration-gradient LiNi$_{0.83}$Co$_{0.07}$Mn$_{0.10}$O$_2$ cathode material showed improved cycling stability compared with the homogeneous LiNi$_{0.9}$Co$_{0.05}$Mn$_{0.05}$O$_2$ (Figure 11d). Unfortunately, the synthesis of concentration-gradient precursors can be synthesized by the batch-type coprecipitation only.
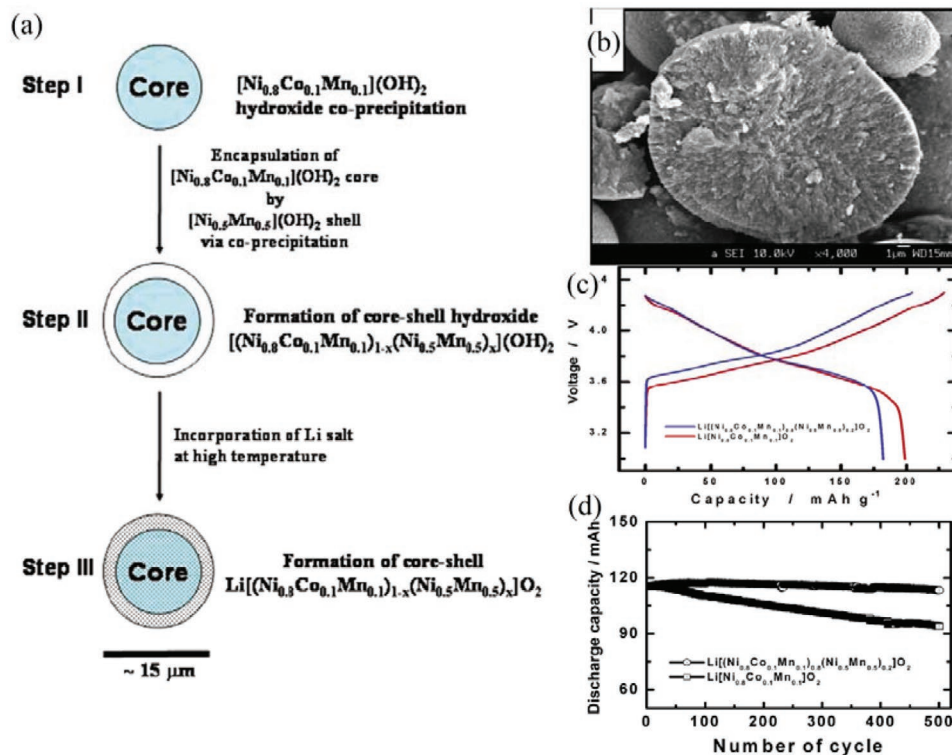

Figure 10. a) Schematic illustration of synthesis process and b) cross-sectional SEM image of core–shell-structured [(Ni$_{0.8}$Co$_{0.1}$Mn$_{0.1}$)$_{0.8}$(Ni$_{0.5}$Mn$_{0.5}$)$_{0.2}$](OH)$_2$, together with the comparison in c) the initial charge–discharge curves and d) cycling performances between the core–shell Li[(Ni$_{0.8}$Co$_{0.1}$Mn$_{0.1}$)$_{0.8}$(Ni$_{0.5}$Mn$_{0.5}$)$_{0.2}$]O$_2$ and LiNi$_{0.8}$Co$_{0.1}$Mn$_{0.1}$O$_2$. Reproduced with permission.[46c] Copyright 2005, American Chemical Society.

**ADVANCED
SCIENCE NEWS**

www.advancedsciencenews.com
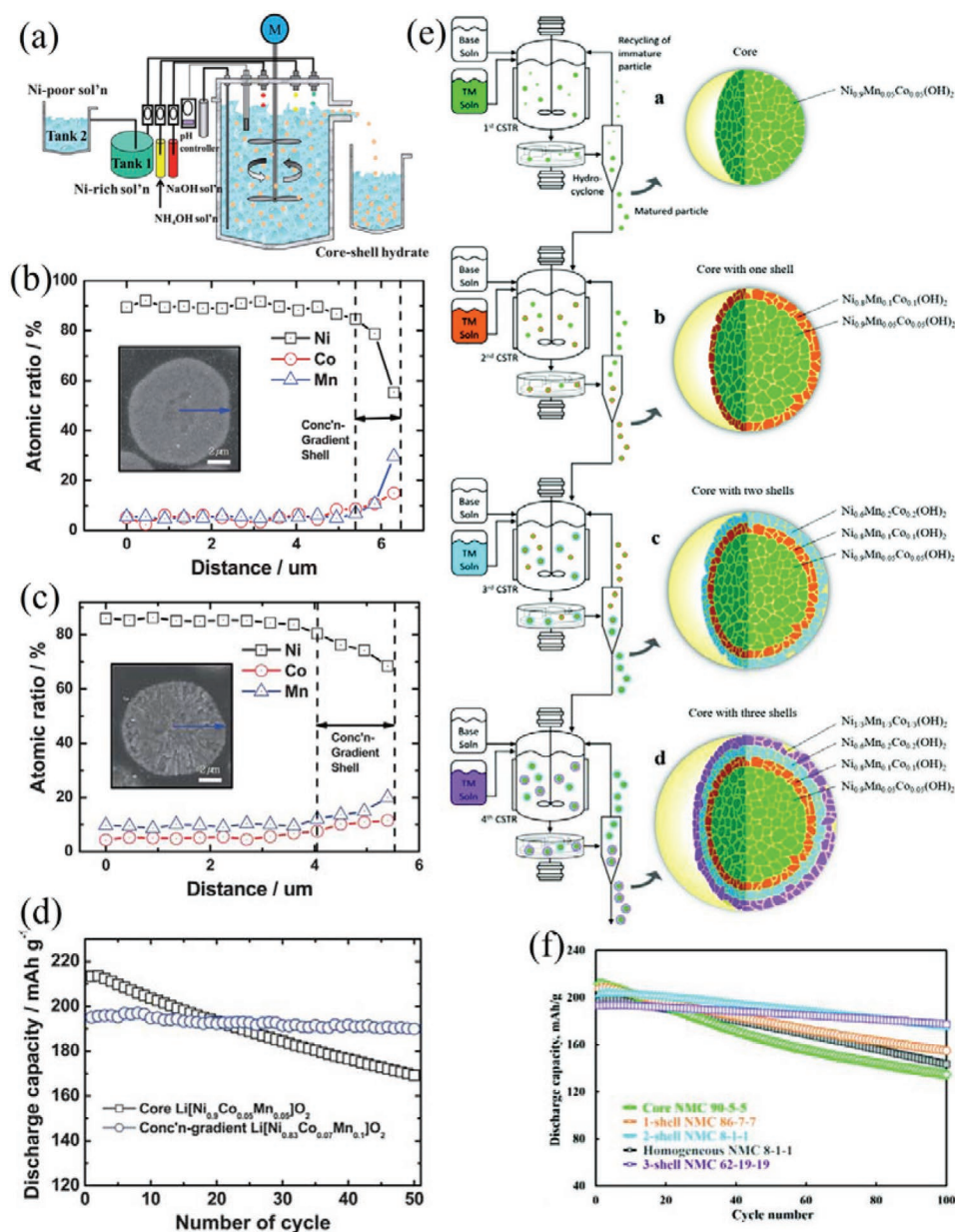
NANO · MICRO

small

www.small-journal.com

Figure 11. a) Schematic illustration of synthesis process of concentration-gradient precursor; the compositional change from the cross-section of b) concentration-gradient $Ni_{0.83}Co_{0.07}Mn_{0.10}(OH)_2$ precursor and c) concentration-gradient $LiNi_{0.83}Co_{0.07}Mn_{0.10}O_2$ cathode material; d) cycling performances of the core $Li[Ni_{0.9}Co_{0.05}Mn_{0.05}]O_2$ and concentration-gradient $LiNi_{0.83}Co_{0.07}Mn_{0.10}O_2$. Reproduced with permission.[47b] Copyright 2011, The Royal Society of Chemistry. e) Schematic illustration of continuous synthesis of digital-gradient precursor, together with f) the cycling performances of the digital-gradient cathodes and homogeneous $LiNi_{0.8}Co_{0.1}Mn_{0.1}O_2$. Reproduced with permission.[60] Copyright 2021, John Wiley and Sons.

Recently, Shin et al.[60] synthesized a core–multishell-structured digital-gradient precursor through a continuous process. In their protocol (Figure 11e), the matured core particles $Ni_{0.9}Mn_{0.05}Co_{0.05}(OH)_2$ discharged from the first reactor were continuously fed into the second one and coated with a $Ni_{0.8}Mn_{0.1}Co_{0.1}(OH)_2$ shell (step a to b). Subsequently, the core particles coated with one shell were discharged from the second reactor and fed into the third one, waiting for the second coating (step b–c). The coating process repeated until the desired core–multishell structure was obtained. After high-temperature lithiation, the obtained cathode material

also showed a concentration-gradient outer layer, which was called "digital-gradient" by the authors. The cathode with 3 shells showed the best cycling performance, but a slightly lower capacity originated from the lower total Ni content (Figure 11f).

5. Summary and Perspectives

In this review, the synthesis, microstructure and electrochemical properties of layered cathode materials are discussed.
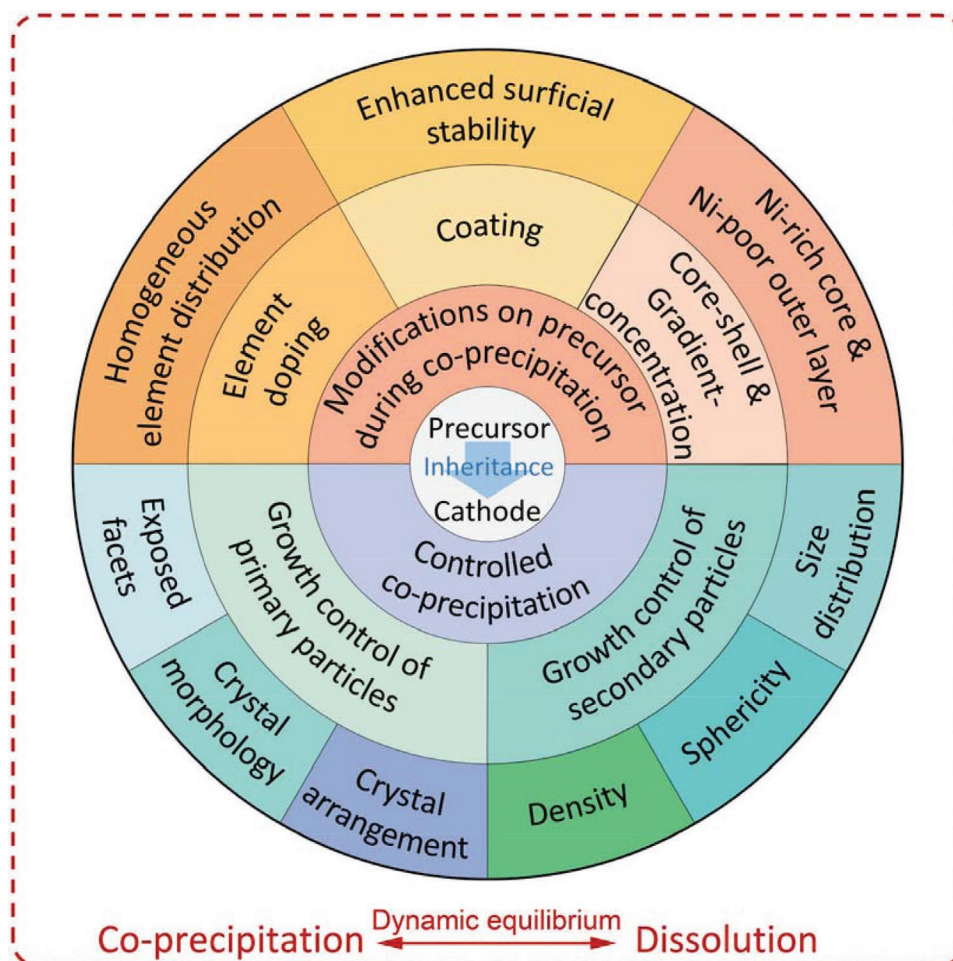
Figure 12. Key parameters in synthesis and modifications of precursors for layered cathode materials.

Principally, the particle growth mechanisms and the parameters in controlling the particle growth of the precursors are comprehensively summarized. Basically, the fundamental for the formation of dense spherical precursor particles is the dynamic equilibrium between coprecipitation and dissolution, which is sensitive to the degree of supersaturation. In addition to the density and sphericity, the arrangement, orientation and exposed facets of the primary particles deserve close attention since they are correlated with the Li^+ diffusion properties and the resistance to inner mechanical stress during charge/discharge for the cathode materials. Furthermore, modifications on hydroxide precursors are also discussed herein. The aforementioned essentials of this review are illustrated in **Figure 12**, which has guidance significance to the development of precursors for layered cathode materials.

Even though substantial progress in the electrochemical performance of Ni-rich layered cathodes has been made by the advances on synthesis, modification, and characterization technologies, the investigations are not so in-depth and comprehensive. For example, it has been proven in many studies that element doping is beneficial to the structural stability of layered cathodes. However, the coordination of dopants in the cathode materials are rarely studied. Meanwhile, the effects of dopants on the particle growth of the precursors, which

indirectly affect the electrochemical behaviors of the final cathodes, are easy to be neglected. Hence, devoting more efforts to fundamental investigations and paying more attentions to the precursors will give new impetus to the development of Ni-rich layered cathodes. In addition, customizing primary particles (e.g., particle morphology, arrangement, mainly exposed facets, etc.) and secondary particles based on specific needs is also a wise strategy. For example, large secondary particles with {001} facets-dominated primary particles are more suitable for long-life batteries, whereas small secondary particles with {010} facets-dominated primary particles are more distinguished in rate capability.

In conclusion, despite the remaining challenges, it is still promising and inspiring to accelerate the moving toward ultrahigh-Ni, even Co-free layered cathodes with great efforts.

Acknowledgements

ADVANCED
SCIENCE NEWS

www.advancedsciencenews.com

NANO · MICRO
small
www.small-journal.com

Conflict of Interest

The authors declare no conflict of interest.

Keywords

[1] a) Z. Ye, L. Qiu, W. Yang, Z. Wu, Y. Liu, G. Wang, Y. Song, B. Zhong, X. Guo, *Chem. – Eur. J.* **2021**, *27*, 4249; b) X. Wang, Y.-L. Ding, Y.-P. Deng, Z. Chen, *Adv. Energy Mater.* **2020**, *10*, 1903864.

[2] W. Lee, S. Muhammad, C. Sergey, H. Lee, J. Yoon, Y.-M. Kang, W.-S. Yoon, *Angew. Chem., Int. Ed.* **2020**, *59*, 2578.

[3] R. J. Brodd, C. Helou, *J. Power Sources* **2013**, *231*, 293.

[4] C. M. Julien, A. Mauger, *Energies* **2020**, *13*, 6363.

[5] a) S. Jamil, A. Bin Yousaf, S. Hee Yoon, D. Suk Han, L. Yang, P. Kasak, X. Wang, *Chem. Eng. J.* **2021**, *416*, 129118; b) G. W. Nam, N.-Y. Park, K.-J. Park, J. Yang, J. Liu, C. S. Yoon, Y.-K. Sun, *ACS Energy Lett.* **2019**, *4*, 2995; c) Y. Lu, Y. Zhang, Q. Zhang, F. Cheng, J. Chen, *Particuology* **2020**, *53*, 1; d) L. de Biasi, A. O. Kondrakov, H. Geßwein, T. Brezesinski, P. Hartmann, J. Janek, *J. Phys. Chem. C* **2017**, *121*, 26163.

[6] a) X. Tan, M. Zhang, J. Li, D. Zhang, Y. Yan, Z. Li, *Ceram. Int.* **2020**, *46*, 21888; b) L.-b. Tang, Y. Liu, H.-x. Wei, C. Yan, Z.-j. He, J.-c. Zheng, *J. Energy Chem.* **2021**, *55*, 114.

[7] a) G.-T. Park, H.-H. Ryu, N.-Y. Park, C. S. Yoon, Y.-K. Sun, *J. Power Sources* **2019**, *442*, 227242; b) Y. Han, X. Cheng, G. Zhao, W. Qiang, B. Huang, *Ceram. Int.* **2021**, *47*, 12104.

[8] a) J. Wang, X. Lu, Y. Zhang, J. Zhou, J. Wang, S. Xu, *J. Energy Chem.* **2022**, *65*, 681; b) P. Pang, X. Tan, Z. Wang, Z. Cai, J. Nan, Z. Xing, H. Li, *Electrochim. Acta* **2021**, *365*, 137380; c) S.-H. Lee, S.-J. Sim, B.-S. Jin, H.-S. Kim, *Mater. Lett.* **2020**, *270*, 127615.

[9] a) K. Liu, Q. Zhang, S. Dai, W. Li, X. Liu, F. Ding, J. Zhang, *ACS Appl. Mater. Interfaces* **2018**, *10*, 34153; b) S. Jamil, G. Wang, L. Yang, X. Xie, S. Cao, H. Liu, B. Chang, X. Wang, *J. Mater. Chem. A* **2020**, *8*, 21306; c) Y. Huang, S. Cao, X. Xie, C. Wu, S. Jamil, Q. Zhao, B. Chang, Y. Wang, X. Wang, *ACS Appl. Mater. Interfaces* **2020**, *12*, 19483.

[10] a) X. Yang, X. Huang, H. Shi, P. Dong, D. Wang, J. Duan, Y. Zhang, *J. Energy Chem.* **2021**, *53*, 379; b) C.-K. Yang, L.-Y. Qi, Z. Zuo, R.-N. Wang, M. Ye, J. Lu, H.-H. Zhou, *J. Power Sources* **2016**, *331*, 487.

[11] Z. Ruan, Y. Zhu, X. Teng, *J. Mater. Sci.* **2016**, *51*, 1400.

[12] D. Li, Z. Peng, W. Guo, C. Yuan, Y. Liu, Y. Zhou, *J. Mater. Sci.* **2007**, *42*, 9221.

[13] a) L. Wang, B. Huang, W. Xiong, M. e. Tong, H. Li, S. Xiao, Q. Chen, Y. Li, J. Yang, *J. Alloys Compd.* **2020**, *844*, 156034; b) A. Ueda, T. Ohzuku, *J. Electrochem. Soc.* **1994**, *141*, 2010.

[14] a) C.-H. Chen, C.-J. Wang, B.-J. Hwang, *J. Power Sources* **2005**, *146*, 626; b) H. Liu, J. Li, Z. Zhang, Z. Gong, Y. Yang, *J. Solid State Electrochem.* **2003**, *7*, 456; c) H. Lu, H. Zhou, A. M. Svensson, A. Fossdal, E. Sheridan, S. Lu, F. Vullum-Bruer, *Solid State Ionics* **2013**, *249–250*, 105.

[15] a) H. M. Wu, J. P. Tu, X. T. Chen, Y. F. Yuan, Y. Li, X. B. Zhao, G. S. Cao, *J. Power Sources* **2006**, *159*, 291; b) P. Yue, Z. Wang, W. Peng, L. Li, H. Guo, X. Li, Q. Hu, Y. Zhang, *Scr. Mater.* **2011**, *65*, 1077; c) P. Yue, Z. Wang, W. Peng, L. Li, W. Chen, H. Guo, X. Li, *Powder Technol.* **2011**, *214*, 279.

[16] a) Y. Zhang, K. Du, Y. Cao, Y. Lu, Z. Peng, J. Fan, L. Li, Z. Xue, H. Su, G. Hu, *J. Power Sources* **2020**, *477*, 228701; b) W.-H. Ryu, S.-J. Lim, W.-K. Kim, H.-S. Kwon, *J. Power Sources* **2014**, *257*, 186.

[17] a) K. K. Cheralathan, N. Y. Kang, H. S. Park, Y. J. Lee, W. C. Choi, Y. S. Ko, Y.-K. Park, *J. Power Sources* **2010**, *195*, 1486; b) K. S. Lee, S. T. Myung, J. S. Moon, Y. K. Sun, *Electrochim. Acta* **2008**, *53*, 6033; c) M. H. Lee, Y. J. Kang, S. T. Myung, Y. K. Sun, *Electrochim. Acta* **2004**, *50*, 939.

[18] a) K. J. Kim, Y. N. Jo, W. J. Lee, T. Subburaj, K. Prasanna, C. W. Lee, *J. Power Sources* **2014**, *268*, 349; b) H. Jia, W. Zhu, Z. Xu, X. Nie, T. Liu, L. Gao, J. Zhao, *Electrochim. Acta* **2018**, *266*, 7.

[19] Y. Shen, Y. Wu, H. Xue, S. Wang, D. Yin, L. Wang, Y. Cheng, *ACS Appl. Mater. Interfaces* **2021**, *13*, 717.

[20] Y. Yang, S. Xu, M. Xie, Y. He, G. Huang, Y. Yang, *J. Alloys Compd.* **2015**, *619*, 846.

[21] M. Bianchini, M. Roca-Ayats, P. Hartmann, T. Brezesinski, J. Janek, *Angew. Chem., Int. Ed.* **2019**, *58*, 10434.

[22] a) S. Zhou, T. Mei, X. Wang, Y. Qian, *Nanoscale* **2018**, *10*, 17435; b) Y. Su, G. Chen, L. Chen, W. Li, Q. Zhang, Z. Yang, Y. Lu, L. Bao, J. Tan, R. Chen, S. Chen, F. Wu, *ACS Appl. Mater. Interfaces* **2018**, *10*, 6407.

[23] F. Fu, G.-L. Xu, Q. Wang, Y.-P. Deng, X. Li, J.-T. Li, L. Huang, S.-G. Sun, *J. Mater. Chem. A* **2013**, *1*, 3860.

[24] A. J. Mahajan, D. J. Kirwan, *J. Phys. D: Appl. Phys.* **1993**, *26*, B176.

[25] F. Cheng, Y. Xin, J. Chen, L. Lu, X. Zhang, H. Zhou, *J. Mater. Chem. A* **2013**, *1*, 5301.

[26] J. Duan, C. Wu, Y. Cao, D. Huang, K. Du, Z. Peng, G. Hu, *J. Alloys Compd.* **2017**, *695*, 91.

[27] a) F. Zhang, S. Lou, S. Li, Z. Yu, Q. Liu, A. Dai, C. Cao, M. F. Toney, M. Ge, X. Xiao, W.-K. Lee, Y. Yao, J. Deng, T. Liu, Y. Tang, G. Yin, J. Lu, D. Su, J. Wang, *Nat. Commun.* **2020**, *11*, 3050; b) M. Ge, S. Wi, X. Liu, J. Bai, S. Ehrlich, D. Lu, W.-K. Lee, Z. Chen, F. Wang, *Angew. Chem., Int. Ed.* **2021**, *60*, 17350; c) Y. Wang, E. Wang, X. Zhang, H. Yu, *Energy Fuels* **2021**, *35*, 1918.

[28] N. Wu, Y. Zhang, Y. Guo, S. Liu, H. Liu, H. Wu, *ACS Appl. Mater. Interfaces* **2016**, *8*, 2723.

[29] J. Ying, C. Wan, C. Jiang, Y. Li, *J. Power Sources* **2001**, *99*, 78.

[30] P. Barai, Z. Feng, H. Kondo, V. Srinivasan, *J. Phys. Chem. B* **2019**, *123*, 3291.

[31] Z. Feng, P. Barai, J. Gim, K. Yuan, Y. A. Wu, Y. Xie, Y. Liu, V. Srinivasan, *J. Electrochem. Soc.* **2018**, *165*, A3077.

[32] S. Bhattacharjee, M. Elimelech, M. Borkovec, *Croat. Chem. Acta* **1998**, *71*, 883.

[33] H. Kim, Y. Kim, *Ceram. Int.* **2020**, *46*, 19476.

[34] Q.-P. Mayra, W.-S. Kim, *Cryst. Growth Des.* **2015**, *15*, 1726.

[35] H. Dong, G. M. Koenig Jr., *J. Mater. Chem. A* **2017**, *5*, 13785.

[36] a) A. van Bommel, J. R. Dahn, *Chem. Mater.* **2009**, *21*, 1500; b) J. Cho, *Chem. Mater.* **2000**, *12*, 3089.

[37] a) Y. Ding, D. Mu, B. Wu, Z. Zhao, R. Wang, *Ceram. Int.* **2020**, *46*, 9436; b) L. Liang, K. Du, Z. Peng, Y. Cao, J. Duan, J. Jiang, G. Hu, *Electrochim. Acta* **2014**, *130*, 82; c) M. Noh, J. Cho, *J. Electrochem. Soc.* **2013**, *160*, A105.

[38] a) Y. Kim, D. Kim, *ACS Appl. Mater. Interfaces* **2012**, *4*, 586; b) K. He, Z. Ruan, X. Teng, Y. Zhu, *Mater. Res. Bull.* **2017**, *90*, 131.

[39] J. C. Masy, M. Cournil, *Chem. Eng. Sci.* **1991**, *46*, 693.

[40] D. K. Thai, Q.-P. Mayra, W.-S. Kim, *Powder Technol.* **2015**, *274*, 5.

[41] Q. Zhu, H. Xiao, R. Zhang, S. Geng, Q. Huang, *Electrochim. Acta* **2019**, *318*, 1.

[42] S. Lee, C.-H. Lee, W.-S. Kim, *J. Cryst. Growth* **2013**, *373*, 32.

[43] a) A. Ochieng, M. S. Onyango, A. Kumar, K. Kiriamiti, P. Musonge, *Chem. Eng. Process.* **2008**, *47*, 842; b) Q. Zhu, H. Xiao, A. Chen, S. Geng, Q. Huang, *Chin. J. Chem. Eng.* **2019**, *27*, 993.

[44] a) L. Cheng, B. Zhang, S.-L. Su, L. Ming, Y. Zhao, X.-X. Tan, *J. Solid State Chem.* **2021**, *297*, 122045; b) Q. Zhang, Y. Su, L. Chen, Y. Lu, L. Bao, T. He, J. Wang, R. Chen, J. Tan, F. Wu, *J. Power Sources* **2018**,

ADVANCED
SCIENCE NEWS
www.advancedsciencenews.com

NANO · MICRO
small
www.small-journal.com

396, 734; c) H. Zhou, F. Zhou, Y. Liu, J. Kong, C. Jin, X. Wu, *J. Alloys Compd.* **2020**, *816*, 152563.

[45] a) B. Huang, X. Li, Z. Wang, H. Guo, L. Shen, J. Wang, *J. Power Sources* **2014**, *252*, 200; b) B. Huang, X. Li, Z. Wang, H. Guo, Z. He, R. Wang, J. Wang, X. Xiong, *Mater. Lett.* **2014**, *115*, 49.

[46] a) Y.-K. Sun, S. T. Myung, H.-S. Shin, Y. S. Bae, C. S. Yoon, *J. Phys. Chem. B* **2006**, *110*, 6810; b) Y. K. Sun, S. T. Myung, B. C. Park, K. Amine, *Chem. Mater.* **2006**, *18*, 5159; c) Y. K. Sun, S. T. Myung, M.-H. Kim, J. Prakash, K. Amine, *J. Am. Chem. Soc.* **2005**, *127*, 13411.

[47] a) H.-J. Noh, S.-T. Myung, H.-G. Jung, H. Yashiro, K. Amine, Y.-K. Sun, *Adv. Funct. Mater.* **2013**, *23*, 1028; b) Y.-K. Sun, B.-R. Lee, H.-J. Noh, H. Wu, S.-T. Myung, K. Amine, *J. Mater. Chem.* **2011**, *21*, 10108; c) G. M. Koenig, I. Belharouak, H. Deng, Y.-K. Sun, K. Amine, *Chem. Mater.* **2011**, *23*, 1954; d) Y.-K. Sun, D.-H. Kim, C. S. Yoon, S.-T. Myung, J. Prakash, K. Amine, *Adv. Funct. Mater.* **2010**, *20*, 485; e) Y.-K. Sun, S.-T. Myung, B.-C. Park, J. Prakash, B. Ilias, K. Amine, *Nat. Mater.* **2009**, *8*, 320.

[48] a) Y.-M. Choi, S.-I. Pyun, S.-I. Moon, *Solid State Ionics* **1996**, *89*, 43; b) J. Zheng, Y. Ye, T. Liu, Y. Xiao, C. Wang, F. Wang, F. Pan, *Acc. Chem. Res.* **2019**, *52*, 2201; c) G. Sun, X. Yin, W. Yang, A. Song, C. Jia, W. Yang, Q. Du, Z. Ma, G. Shao, *Phys. Chem. Chem. Phys.* **2017**, *19*, 29886.

[49] C. Zhang, M. Liu, G. Pan, S. Liu, D. Liu, C. Chen, J. Su, T. Huang, A. Yu, *ACS Appl. Energy Mater.* **2018**, *1*, 4374.

[50] a) K.-J. Park, H.-G. Jung, L.-Y. Kuo, P. Kaghazchi, C. S. Yoon, Y.-K. Sun, *Adv. Energy Mater.* **2018**, *8*, 1801202; b) P. Oh, J. Yun, S. Park, G. Nam, M. Liu, J. Cho, *Adv. Energy Mater.* **2021**, *11*, 2003197; c) L. Zou, J. Li, Z. Liu, G. Wang, A. Manthiram, C. Wang, *Nat. Commun.* **2019**, *10*, 3447.

[51] a) J. U. Choi, N. Voronina, Y.-K. Sun, S.-T. Myung, *Adv. Energy Mater.* **2020**, *10*, 2002027; b) D. Kitsche, S. Schweidler, A. Mazilkin, H. Geßwein, F. Fauth, E. Suard, P. Hartmann, T. Brezesinski, J. Janek, M. Bianchini, *Mater. Adv.* **2020**, *1*, 639.

[52] a) H. Yu, H. Zhu, Z. Yang, M. Liu, H. Jiang, C. Li, *Chem. Eng. J.* **2021**, *412*, 128625; b) L. Luo, D. Wang, Z. Zhou, P. Dong, S. Yang, J. Duan, Y. Zhang, *ACS Appl. Mater. Interfaces* **2021**, *13*, 45068; c) B. Chu, L. You, G. Li, T. Huang, A. Yu, *ACS Appl. Mater. Interfaces* **2021**, *13*, 7308; d) U.-H. Kim, N.-Y. Park, G.-T. Park, H. Kim, C. S. Yoon, Y.-K. Sun, *Energy Storage Mater.* **2020**, *33*, 399; e) M. Jeong, H. Kim, W. Lee, S.-J. Ahn, E. Lee, W.-S. Yoon, *J. Power Sources* **2020**, *474*, 228592; f) G. Shang, Y. Tang, Y. Lai, J. Wu, X. Yang, H. Li, C. Peng, J. Zheng, Z. Zhang, *J. Power Sources* **2019**, *423*, 246.

[53] a) C. Zhang, J. Wan, Y. Li, S. Zheng, K. Zhou, D. Wang, D. Wang, C. Hong, Z. Gong, Y. Yang, *J. Mater. Chem. A* **2020**, *8*, 6893; b) H.-H. Ryu, G.-T. Park, C. S. Yoon, Y.-K. Sun, *J. Mater. Chem. A* **2019**, *7*, 18580; c) Q. Liu, K. Du, H. Guo, Z.-d. Peng, Y.-b. Cao, G.-r. Hu, *Electrochim. Acta* **2013**, *90*, 350.

[54] a) W. Cho, Y. J. Lim, S.-M. Lee, J. H. Kim, J.-H. Song, J.-S. Yu, Y.-J. Kim, M.-S. Park, *ACS Appl. Mater. Interfaces* **2018**, *10*, 38915; b) L. Tian, H. Yuan, Q. Shao, S. D. A. Zaidi, C. Wang, J. Chen, *Ionics* **2020**, *26*, 4937.

[55] a) L. Qiu, M. Zhang, Y. Ming, Y. Song, Z. Wu, Q. Xu, T. Chen, G. Wang, Y. Liu, F. He, J. Zhang, H. Yan, B. Zhang, W. Xiang, X.-D. Guo, E. Yang, *Chem. Eng. Sci.* **2021**, *233*, 116337; b) C. Xu, W. Yang, W. Xiang, Z. Wu, Y. Song, G. Wang, Y. Liu, H. Yan, B. Zhang, B. Zhong, X. Guo, *Ind. Eng. Chem. Res.* **2020**, *59*, 22549.

[56] a) S.-J. Sim, S.-H. Lee, B.-S. Jin, H.-S. Kim, *J. Power Sources* **2021**, *481*, 229037; b) B. Huang, G. Li, Z. Pan, X. Su, L. An, *J. Alloys Compd.* **2019**, *773*, 519; c) S. Zhao, Y. Zhu, Y. Qian, N. Wang, M. Zhao, J. Yao, Y. Xu, *Mater. Lett.* **2020**, *265*, 127418; d) D. Weber, Đ. Tripković, K. Kretschmer, M. Bianchini, T. Brezesinski, *Eur. J. Inorg. Chem.* **2020**, *2020*, 3117.

[57] a) Y.-S. Lee, D. Ahn, Y.-H. Cho, T. E. Hong, J. Cho, *J. Electrochem. Soc.* **2011**, *158*, A1354; b) L. Tang, G. Li, P. Xiao, X. Chen, W. Yang, *RSC Adv.* **2019**, *9*, 9079; c) A. L. Lipson, B. J. Ross, J. L. Durham, D. Liu, M. LeResche, T. T. Fister, L. Liu, K. Kim, *ACS Appl. Energy Mater.* **2021**, *4*, 1972; d) J. S. Lee, Y. J. Park, *ACS Appl. Mater. Interfaces* **2021**, *13*, 38333; e) Y. Cho, Y.-S. Lee, S.-A. Park, Y. Lee, J. Cho, *Electrochim. Acta* **2010**, *56*, 333.

[58] a) X. Lu, X. Li, Z. Wang, H. Guo, G. Yan, X. Yin, *Appl. Surf. Sci.* **2014**, *297*, 182; b) G. Li, L. Qi, P. Xiao, Y. Yu, X. Chen, W. Yang, *Electrochim. Acta* **2018**, *270*, 319; c) Y.-C. Li, W. Xiang, Y. Xiao, Z.-G. Wu, C.-L. Xu, W. Xu, Y.-D. Xu, C. Wu, Z.-G. Yang, X.-D. Guo, *J. Power Sources* **2019**, *423*, 144.

[59] a) Y. Liu, H. Wu, Y. Wang, K. Li, S. Yin, J. R. Dahn, *J. Electrochem. Soc.* **2021**, *167*, 160556; b) R. Tian, J. Su, Z. Ma, D. Song, X. Shi, H. Zhang, C. Li, L. Zhang, *Electrochim. Acta* **2020**, *337*, 135769; c) Y. Sun, W. Lv, P. Fu, Y. Song, D. Song, X. Shi, H. Zhang, C. Li, L. Zhang, D. Wang, *Chem. Eng. J.* **2020**, *400*, 125821; d) S. Maeng, Y. Chung, S. Min, Y. Shin, *J. Power Sources* **2020**, *448*, 227395; e) N. Zhang, N. Zaker, H. Li, A. Liu, J. Inglis, L. Jing, J. Li, Y. Li, G. A. Botton, J. R. Dahn, *Chem. Mater.* **2019**, *31*, 10150.

[60] Y. Shin, S. Maeng, Y. Chung, G. K. Krumdick, S. Min, *Small* **2021**, *17*, 2100040.

Bin Huang is an associate professor in the College of Chemistry and Bioengineering, Guilin University of Technology (Guilin, China). He received his Ph.D. degree in Electrochemical Engineering from School of Metallurgy and Environment, Central South University (Changsha, China) in 2016. He worked as a postdoctoral fellow at The Hong Kong Polytechnic University from 2017 to 2018. His current research is focused on processing and modification of electrode materials for lithium- & sodium-ion batteries.

Lei Cheng is the Executive Vice-President of the Research & Development Department of Zhejiang Power New Energy Co. Ltd. (Shaoxing, China). He is in charge of the development of precursors for layered cathode materials for lithium-ion batteries. He received his Ph.D. degree from School of Metallurgy and Environment, Central South University (Changsha, China) in 2021.

Guozhong Cao is Boeing-Steiner professor of Materials Science and Engineering, professor of Chemical Engineering and adjunct professor of Mechanical Engineering at the University of Washington, Seattle, WA. He is one of the Thomson Reuters Highly Cited Researchers with a total citation of 42 000 and an h-index of 102. His current research focused on chemical processing of nanomaterials for solar cells, batteries, and supercapacitors as well as actuators and sensors.